[redacted] Copy 577

NASA TM X-429

NASA TM X-429

GPO PRICE $ _____

OTS PRICE(S) $ _____

Hard copy (HC) 2.00

Microfiche (MF) .50

TECHNICAL MEMORANDUM

X-429

TRANSONIC AERODYNAMIC CHARACTERISTICS OF A VARIABLE-SWEEP AIRPLANE CONFIGURATION HAVING A 12-PERCENT-THICK WING AND AN INBOARD PIVOT LOCATION

By Ralph P. Bielat and P. Kenneth Pierpont

Langley Research Center
Langley Field, Va.

[redacted]

NATIONAL AERONAUTICS AND SPACE ADMINISTRATION

WASHINGTON December 1960

[redacted]

NATIONAL AERONAUTICS AND SPACE ADMINISTRATION

TECHNICAL MEMORANDUM X-429

TRANSONIC AERODYNAMIC CHARACTERISTICS OF A VARIABLE-SWEEP AIRPLANE CONFIGURATION HAVING A 12-PERCENT-THICK WING AND AN INBOARD PIVOT LOCATION *

By Ralph P. Bielat and P. Kenneth Pierpont

SUMMARY

An investigation has been made in the Langley 8-foot transonic pressure tunnel to determine the aerodynamic characteristics of an airplane configuration capable of low-level supersonic attack. The configuration incorporated a variable-sweep wing, and the investigation was made with the wing swept back 16°, 75°, and 94°.

The wind-tunnel results indicated that the zero-lift drag rise of the configuration with a maximum wing sweep of 94° was only slightly lower than that for a wing sweep of 75°, but the large reduction in lift-curve slope would reduce the gust accelerations. For a wing sweep of 16°, the maximum lift-drag ratio occurred near a Mach number of 0.6. During transition from the low sweep to high sweep, very large changes in aerodynamic center were measured. This large variation in stability for this configuration resulted primarily from the inboard pivot location and the limited amount of fixed area forward of the pivot point.

Author

INTRODUCTION

The present investigation is part of a more general research program intended to evaluate the aerodynamic characteristics of variable-sweep airplane configurations capable of low-level supersonic attack.

---

* Title, Unclassified.

[redacted]

Two configurations of this program, in which some 10 configurations were considered, are reported in reference 1. These results compared the aerodynamic characteristics at transonic speeds of configurations with an inboard and with an outboard wing-pivot location. The inboard pivot is conducive to low pivot structural weight and low skin-friction drag; whereas, the outboard pivot provides a means for limiting the aerodynamic-center travel for a large range of wing-sweep angles. Both models of reference 1 were designed in accordance with the transonic area-rule concept of reference 2 and employed axisymmetrical translating spike inlets.

In cooperation with the National Aeronautics and Space Administration, Wright Air Development Division, U.S. Air Force, has proposed a configuration which combines the advantages of the improved angle-of-attack pressure recovery of a two-dimensional sweptback inlet and the low structural weight of the inboard pivot. This configuration was also designed according to the transonic area-rule concept of reference 2. Tests of the model, which is referred to as configuration XA, are reported herein. Results were obtained in the Langley 8-foot transonic pressure tunnel at Mach numbers ranging from 0.60 to 0.96 for the wings swept back 16° and from 0.60 to 1.20 for the wings swept 75° and the maximum sweep of 94°.

SYMBOLS

The data are referred to the wind axes and are based on an area of 1 square foot and a reference chord of 1 foot. The pitching moments have been referred to an axis which is located at the wing-pivot axis. (See fig. 1.) The coefficients and symbols used herein are defined as follows:

A	cross-sectional area, sq ft
c	reference chord, 1.00 ft
$C_{A,i}$	internal axial-force coefficient, $\frac{\text{Internal axial force}}{qS}$
C_D	drag coefficient, $\frac{\text{Drag}}{qS}$
$C_{D,b}$	base-drag coefficient, $\frac{(p_b - p_\infty)A_b}{qS}$
$C_{D,o}$	drag coefficient at zero lift

[redacted]

$\Delta C_{D,o}$	incremental drag rise at zero lift, $(C_{D,o})_M - (C_{D,o})_{M=0.80}$
C_L	lift coefficient, $\frac{\text{Lift}}{qS}$
$C_{L,(L/D)_{max}}$	lift coefficient for $(L/D)_{max}$
C_{L_α}	lift-curve slope, $dC_L/d\alpha$, per deg
C_m	pitching-moment coefficient, $\frac{\text{Pitching moment}}{qSc}$
l	length of fuselage from nose to engine exhaust, 76.83 ft, full scale
L/D	lift-drag ratio
M	free-stream Mach number
p	pressure, lb/sq ft
p_t	stagnation pressure, atm
q	free-stream dynamic pressure, $\frac{1}{2}\rho V^2$, lb/sq ft
R	Reynolds number based on c = 1.00 ft
S	reference area, 1.00 sq ft
V	velocity, ft/sec
w	mass rate of air flow, ρAV, slugs/sec
w/w_∞	mass-flow ratio based on inlet capture area, A_c = 13.4 sq ft, full scale
x	distance from nose of fuselage, ft
α	angle of attack referred to fuselage reference line, deg
δ_h	stabilizer incidence referred to fuselage reference line, positive when trailing edge is down, deg

ρ mass density of air, slugs/cu ft

Λ sweep angle of wing leading edge, deg

Subscripts:

b base of model including sting and sting clearance

c capture

∞ free stream

max maximum

MODEL DESCRIPTION

The general arrangement of configuration XA is shown in figure 1 and photographs of the 1/24-scale wind-tunnel model having three different sweep angles (that is, $\Lambda = 16^\circ$, 75°, and 94°) are shown in figure 2. The configuration has a maximum frontal area of 51.7 square feet when 8.2 square feet are assumed to be captured by the inlets at $M = 1.2$. The airplane wetted area for the maximum sweep condition is estimated to be 2,950 square feet and the plan projected area is 960 square feet. Decreasing the wing sweep to $\Lambda = 16^\circ$ increases the wetted area to 3,380 square feet. The inboard wing pivot is located at 49.5 percent of the fuselage length and laterally is adjacent to the outer wall of the rectangular engine-air duct to permit sufficient depth for the necessary pivot structure. The wing section outboard of the pivot is an NACA 23012 airfoil perpendicular to the leading edge. The horizontal- and vertical-tail sections are 3-percent-thick circular arcs parallel to the free stream.

The total cross-sectional area distribution developed from the 1/24-scale model templates for $M = 1.0$ has been plotted in figure 3 and is compared with that for a Sears-Haack body of revolution having the same overall length and effective diameter and with the maximum area at the midlength. In developing the areas rearward from the inlet, an area equivalent to 61 percent of the maximum capture area was subtracted to account for the required engine air flow. The resulting fineness ratio of the equivalent body was 10.5.

The model, constructed of plastic-impregnated fiberglass on a steel strongback to a scale of 1/24, was provided with three interchangeable wing panels so that wing sweeps of 16°, 75°, and the maximum of 94° could be tested. In each case the juncture of the inner and outer panel

consisted of a step and was simulated on the model as shown in figure 2. The inlets, which are two-dimensional external-compression types with variable second ramp and throat, were provided in the model with an insert wedge of the appropriate initial angle to cause the throat to choke near the required mass-flow ratio for a Mach number of 1.2. (See fig. 1.) The measured variation of mass-flow ratio, based upon the full-scale inlet capture area of 13.4 square feet, is shown in figure 4. The experimental values are shown to be within a few percent of $\frac{W}{W_\infty} = 0.61$ previously mentioned in connection with the area distribution curve.

APPARATUS AND PROCEDURES

Tunnel

The investigation was made in the Langley 8-foot transonic pressure tunnel. This facility is rectangular in cross section with the upper and lower walls slotted longitudinally to allow continuous operation through the transonic speed range with negligible effects of choking and blockage. The stagnation temperature and dewpoint were maintained at values to preclude shock condensation effects. The tunnel was operated at the highest stagnation pressures consistent with the load limits of the model and balance. For $\Lambda = 16^\circ$, therefore, the stagnation pressure was about one-fourth atmosphere; for $\Lambda = 75^\circ$, one-half atmosphere; and for $\Lambda = 94^\circ$, the stagnation pressure was maintained at one atmosphere. The Reynolds number based on a characteristic length of 1 foot is shown in figure 5 as a function of test Mach number for the three stagnation pressures maintained. The Reynolds number varied from 0.83×10^6 to 1.06×10^6 for the lowest sweep angle and from 3.17×10^6 to 4.25×10^6 for the maximum sweep configuration.

Measurements

Lift, drag, and pitching moment were determined by means of an electrical strain-gage balance located inside the fuselage. The measurements were taken over an angle-of-attack range for Mach numbers ranging from 0.60 to 0.96 for the configuration with the wings swept back 16° and from 0.60 to 1.20 for the configurations with the wings swept back 75° and 94°. Total-pressure and static-pressure measurements were taken at the exit of one duct to determine the mass-flow and internal axial-force coefficient. Duct flow was assumed to be symmetrical. The pressure in the balance chamber was measured and the same pressure was assumed to act over the small base area surrounding the sting and the duct exits.

All tests were conducted with fixed transition on the model according to the methods described in reference 3. The transition was fixed by applying 0.10-inch-wide strips of No. 80 carborundum grains around the fuselage 3 inches back from the nose, at the leading edge of the inlets, at the 10-percent-chord location (perpendicular to the leading edge) of both surfaces of the wings for the wings swept back 16° and 75° only, and at the 10-percent-chord location (streamwise) on all surfaces of the horizontal and vertical tails.

Corrections and Accuracy

No corrections to the free-stream Mach number and dynamic pressure for the effects of model and wake blockage are necessary for tests in the slotted test section of the Langley 8-foot transonic pressure tunnel. (See ref. 4.) There is a range of Mach numbers above a Mach number of 1.00 where the data are affected by reflected compressions and expansions from the test-section boundary. From considerations of the results of reference 5, it is believed that for Mach numbers up to approximately 1.03 the effects of these disturbances on the measurements made in the present investigation would be negligible. No test data, however, are presented in the range ($M > 1.03$ and $M < 1.15$) where the reflected boundary disturbances impinged upon the model.

The drag coefficient C_D was corrected by adjusting the static pressure at the base and balance chamber of the model to the free-stream value. Typical plots of the base-drag coefficient against angle of attack are given in figure 6(a). The drag coefficient also includes the correction for the internal axial-force coefficient $C_{A,i}$ due to the flow through the ducts. The variation of the internal axial-force coefficient with angle of attack is shown in figure 6(b). This axial-force coefficient is the total value for both nacelles.

No sting interference corrections have been made to the data except to the extent of the partial correction for sting interference inherent in the base-pressure correction.

The angle of attack has been corrected for flow angularity and for the deflection of the sting support under load. The angle of attack is estimated to be accurate to within ±0.1°.

The estimated accuracy of the data based primarily on the static calibrations and the repeatability of the data is as follows:

C_L	±0.002
C_D	±0.0004
C_m	±0.002
M	±0.003

RESULTS AND DISCUSSION

Presentation of Results

The results of this investigation are presented in the following figures:

Drag Characteristics

The effects of wing sweep on the zero-lift drag characteristics are summarized in figure 10. An increase in wing sweep from 16° to 94° increased the drag-rise Mach number from 0.80 to approximately 0.98. Although sizable reductions in zero-lift drag occurred at transonic speeds with increases in wing sweep from 16° to 75° (fig. 10), the zero-lift

drag-rise characteristics of the configuration with the maximum wing sweep of 94° was only slightly lower than the configuration with $\Lambda = 75°$. (See fig. 11.)

The untrimmed lift-drag ratio characteristics for the configurations with wing-sweep angles of 16° and 75° are shown in figure 12 and the variation of untrimmed $(L/D)_{max}$ and lift coefficient for $(L/D)_{max}$ with Mach number for the same configurations is given in figure 13. Large reductions in the values of $(L/D)_{max}$ at Mach numbers above 0.60 occurred for the configuration with the wing swept 16°. For this wing sweep and at $M = 0.60$, additional data were obtained to determine the cause of the large discontinuities in the basic aerodynamic characteristics shown by the data of figure 7, since the discontinuities occurred at lift coefficients which may have affected $(L/D)_{max}$. First, the large step at the juncture of the inner and outer wing panel, shown in figure 2, was faired smooth. Insignificant changes in overall characteristics are indicated in figure 7 to have resulted from this modification; however, the zero-lift drag decreased about 0.0010. Then, with the step faired, the Reynolds number was increased from about 0.8×10^6 to 3.2×10^6 by increasing the stagnation pressure from 0.25 to 1.0 atmosphere. This Reynolds number increase resulted in the elimination of the discontinuities and an increase in $(L/D)_{max}$ from 10.5 to 13.1 shown in figures 12 and 13. Since the phenomenon is believed to be a laminar separation on the wing outer panel because of low Reynolds number, similar improvement but of decreased magnitude could be expected in $(L/D)_{max}$ for the data shown at $M = 0.80$. Increasing the wing sweep from 16° to 75° was accompanied by a large decrease in $(L/D)_{max}$ at $M = 0.60$; however, for Mach numbers above 0.80, the maximum lift-drag ratio characteristics were superior to that for the configuration with $\Lambda = 16°$.

Longitudinal Stability Characteristics

The effects of wing sweep and Mach number on the lift-curve slope characteristics measured near zero lift are shown in figure 14. A large "bucket" in the lift-curve slope characteristics above the force-break Mach number is indicated for the wing swept back 16° which is typical of wings of large aspect ratio and thickness ratio. Increasing the wing-sweep angle from 16° to 94° produced large reductions in the lift-curve slope and decreased the variation with Mach number. The low values of C_{L_α} for the wing swept back 94° would be beneficial from a gust-acceleration standpoint for high-speed, low-level flight.

There was no longitudinal instability indicated over the lift-coefficient range tested for the three configurations with the horizontal

tail on. (See figs. 7(c), 8(c), and 9(c).) The small positive values of C_m at $C_L = 0$ for the configurations with sweep angles of 16° and 75° would relieve the trimming requirements; whereas, the trimming requirements are increased by the small negative values of C_m at $C_L = 0$ for the configuration with $\Lambda = 94°$ and $\delta_h = 0°$. (See fig. 9(c).)

The aerodynamic-center location x/l for the three wing sweeps tested is shown in figure 15. The wing-pivot axis is also shown for reference. It will be noted that, for a given sweep angle, the variation of the aerodynamic-center location with Mach number was small. However, the variation of the aerodynamic center with wing sweep is very large (approximately 9.2 feet, full scale); therefore, large trim changes and correspondingly large trim drags, would occur during wing transition. In addition large trim drags would be expected during supersonic cruise where relatively large sweep angles would be used.

L
1
2
4
8

The large stability variations with wing sweep are primarily due to the fact that: (1) the inboard pivot location required a large wing panel to be rotated to provide the span desired and (2) the forward location of the pivot limited the size of the fixed area of wing ahead of the pivot. A discussion and bibliography relative to methods of avoiding these stability variations can be found in part II of reference 6.

CONCLUDING REMARKS

An investigation has been made in the Langley 8-foot transonic pressure tunnel to determine the aerodynamic characteristics of an airplane configuration capable of low-level supersonic attack. The configuration incorporated a variable-sweep wing, having a 12-percent-thick wing and a pivot location within the fuselage. Wing sweep angles of 16°, 75°, and 94° were investigated.

The wind-tunnel results have indicated that, although sizable reductions in zero-lift drag occurred at transonic speeds with increases in wing sweep from 16° to 75°, the zero-lift drag-rise characteristics of the configuration with the maximum wing sweep of 94° was only slightly lower than that for the configuration with the wing swept 75°. However, fairly large reductions in gust-induced accelerations would be expected for the maximum sweep angle due to the low lift-curve slope. For the configuration with 16° wing sweep, large reductions in the values of maximum lift-drag ratio at Mach numbers above 0.60 were indicated and are due primarily to the thick wing. The variation of the aerodynamic center with wing sweep is very large (approximately 9.2 feet, full

scale); therefore, large trim changes during transition and large supersonic trim drag penalties would be encountered. The large variation in stability for this particular configuration is due primarily to the fact that the inboard pivot location required a large wing panel to be rotated and the forward pivot location limited the amount of fixed area.

Langley Research Center,
National Aeronautics and Space Administration,
Langley Field, Va., September 13, 1960.

REFERENCES

1. Bielat, Ralph P., Robins, A. Warner, and Alford, William J., Jr.: The Transonic Aerodynamic Characteristics of Two Variable-Sweep Airplane Configurations Capable of Low-Level Supersonic Attack. NASA TM X-304, 1960.

2. Whitcomb, Richard T.: A Study of the Zero-Lift Drag-Rise Characteristics of Wing-Body Combinations Near the Speed of Sound. NACA Rep. 1273, 1956. (Supersedes NACA RM L52H08.)

3. Braslow, Albert L., and Knox, Eugene C.: Simplified Method for Determination of Critical Height of Distributed Roughness Particles for Boundary-Layer Transition at Mach Numbers From 0 to 5. NACA TN 4363, 1958.

4. Wright, Ray H., and Ward, Vernon G.: NACA Transonic Wind-Tunnel Test Sections. NACA Rep. 1231, 1955. (Supersedes NACA RM L8J06.)

5. Wright, Ray H., Ritchie, Virgil S., and Pearson, Albin O.: Characteristics of the Langley 8-Foot Transonic Tunnel With Slotted Test Section. NACA Rep. 1389, 1958. (Supersedes NACA RM L51H10 by Wright and Ritchie and RM L51K14 by Ritchie and Pearson.)

6. Staff of the NASA: Compilation of Papers Summarizing Some Recent NASA Research on Manned Military Aircraft. NASA TM X-420, 1960.

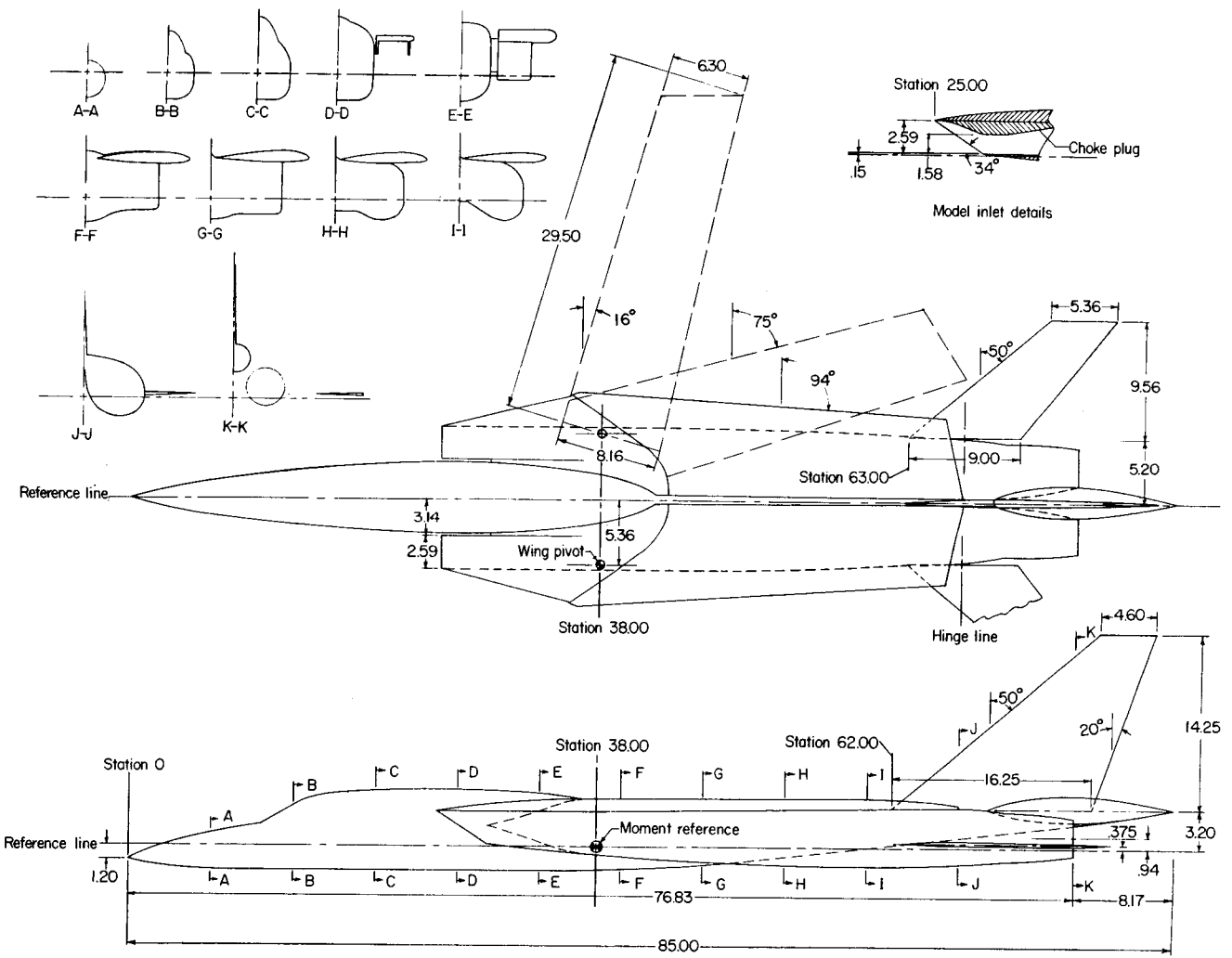

Figure 1.- General arrangement of configuration XA. All dimensions are in feet unless otherwise noted.

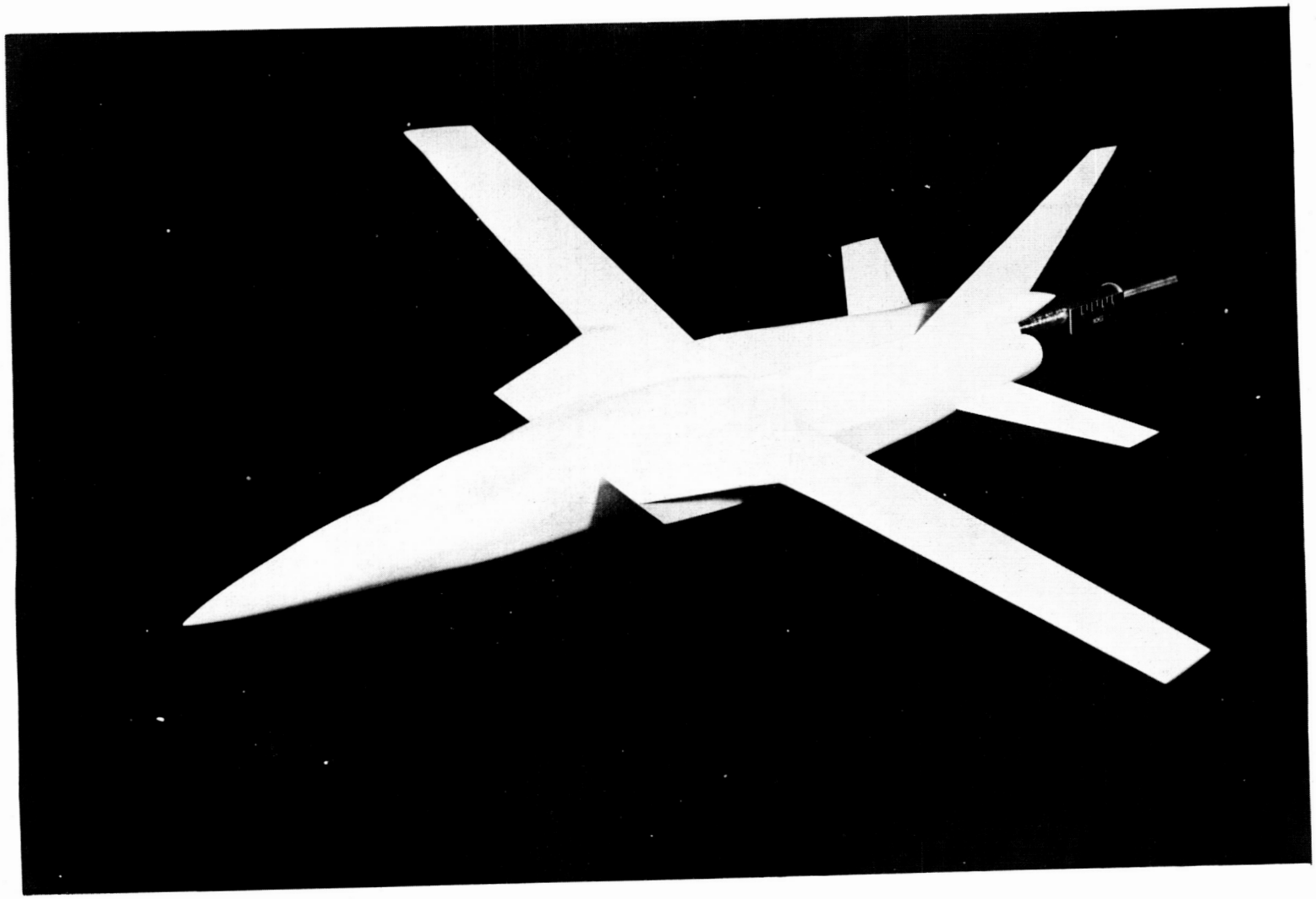

(a) Three-quarter front view. $\Lambda = 16^{\circ}$. L-60-3167

Figure 2.- Configuration XA tested in Langley 8-foot transonic pressure tunnel.

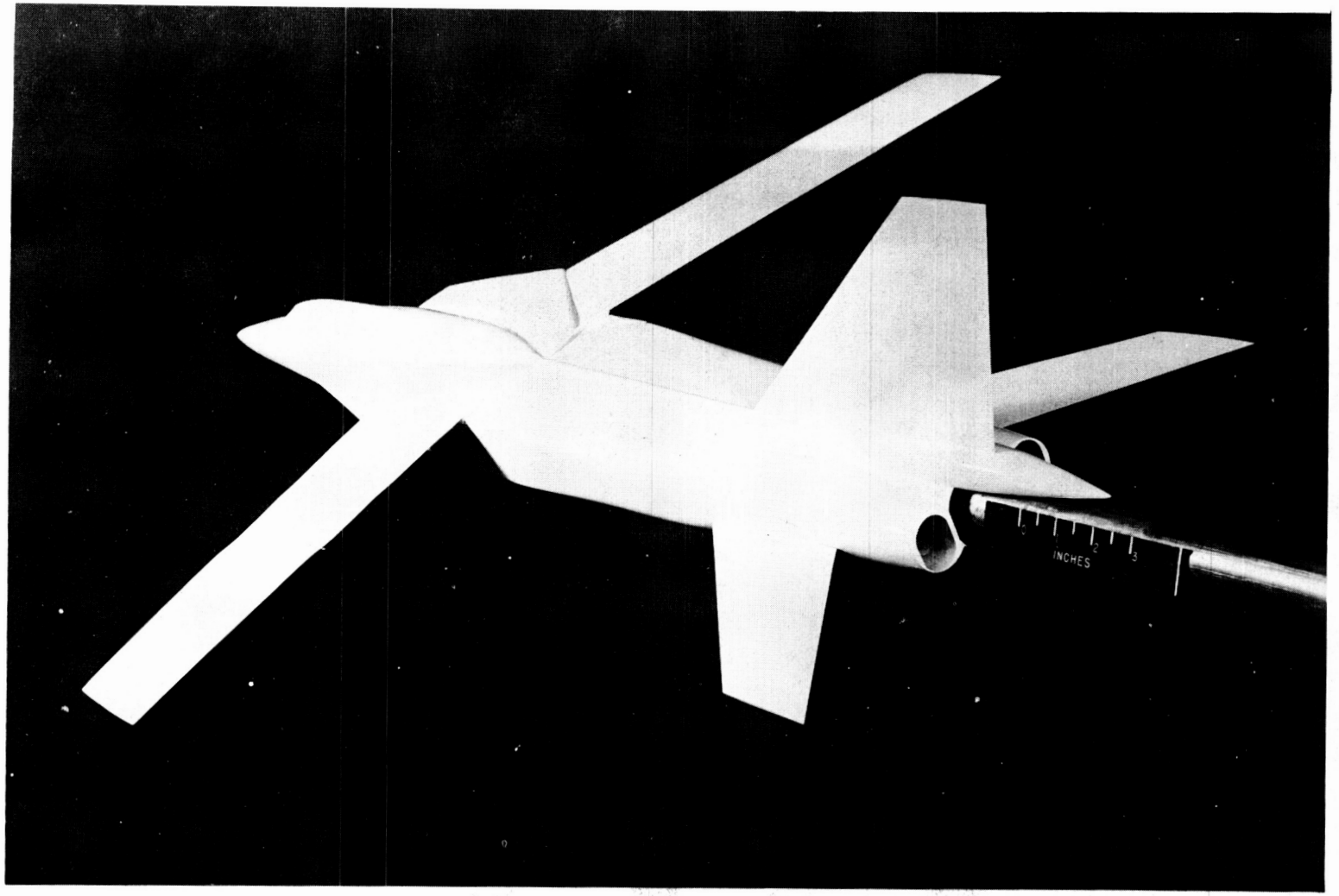

(b) Three-quarter rear view. $\Lambda = 16^{\circ}$.

L-60-3168

Figure 2.- Continued.

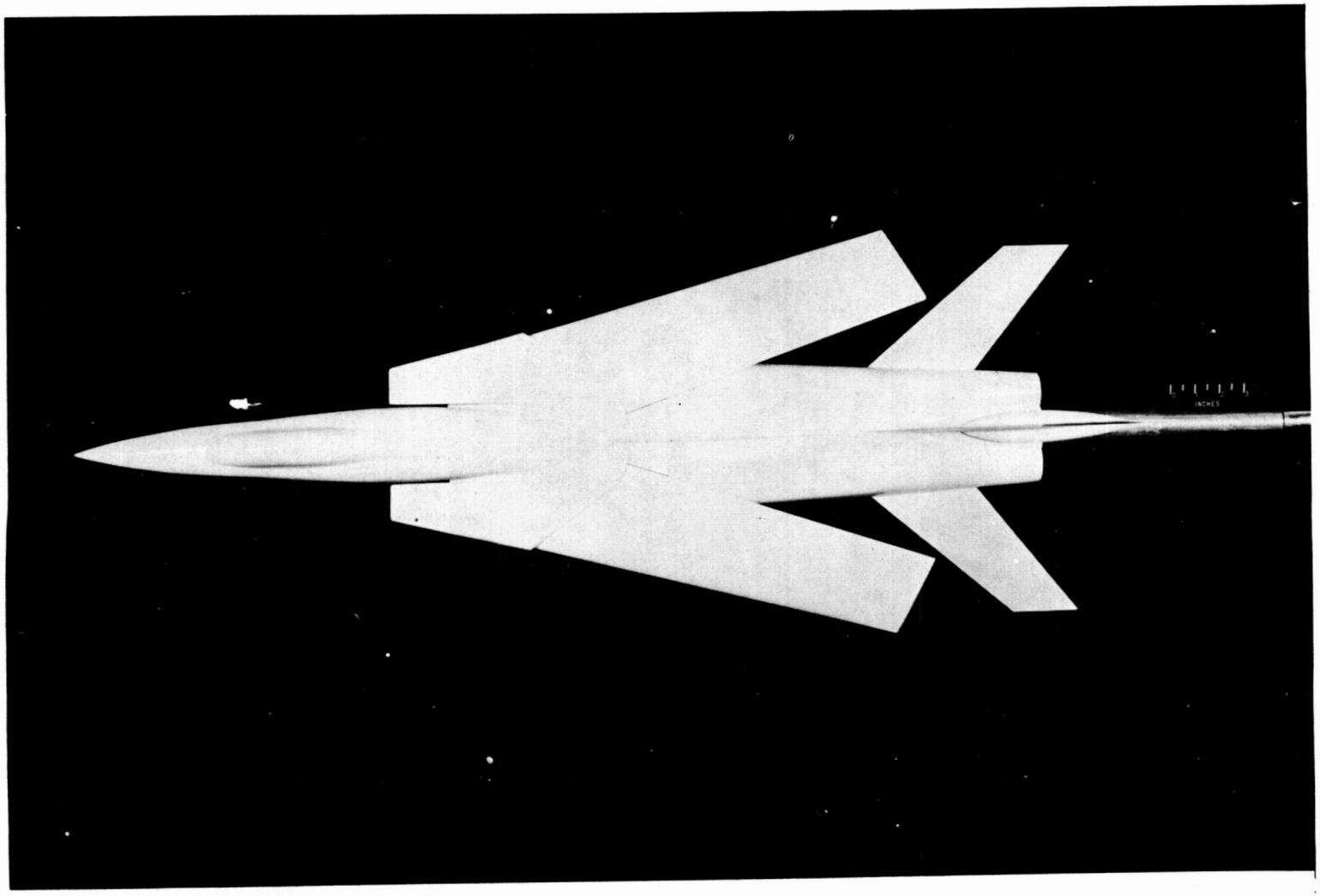

(c) Plan view. $\Lambda = 75^{\circ}$.

L-60-3164

Figure 2.- Continued.

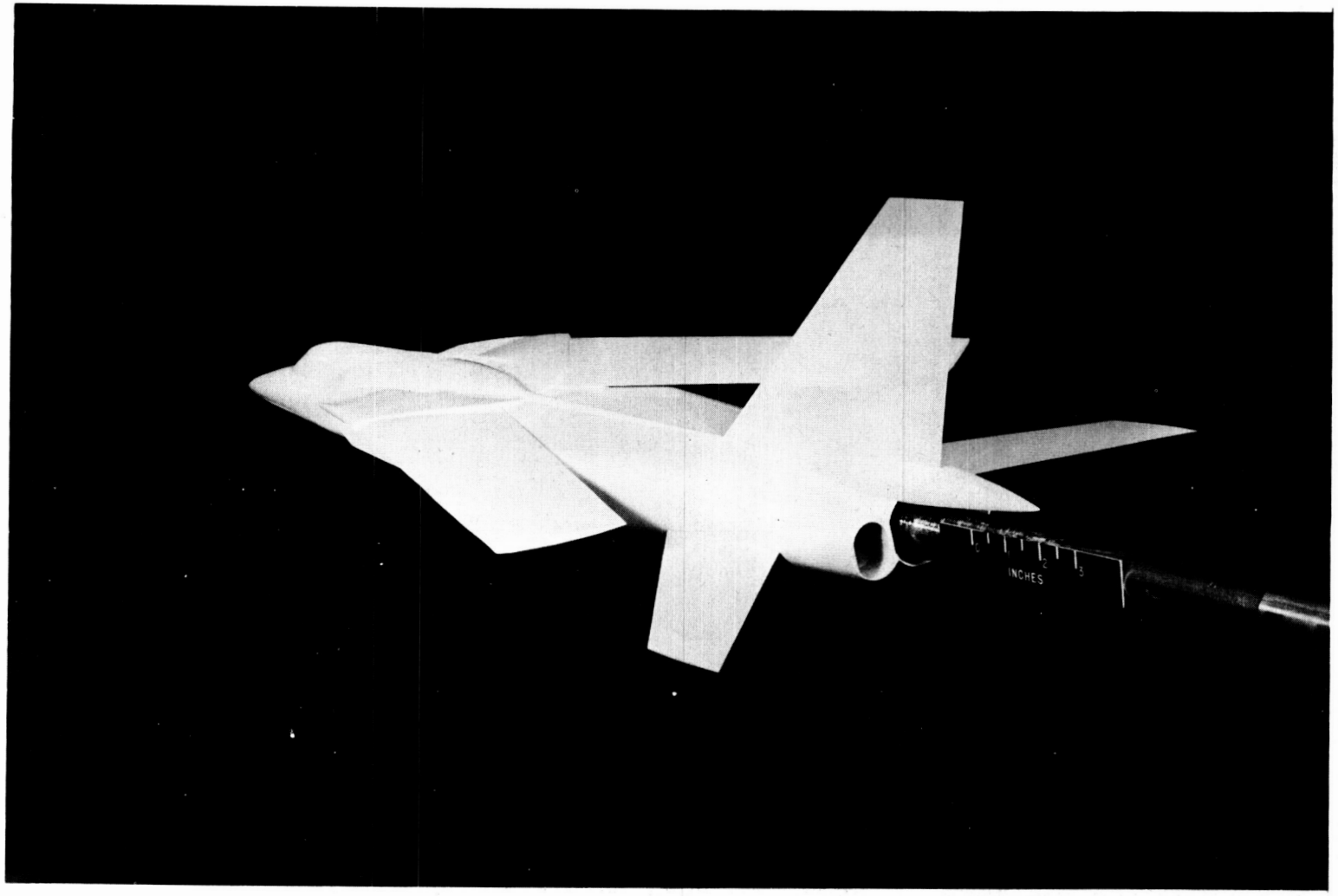

(d) Three-quarter rear view. $\Lambda = 75^{\circ}$. L-60-3165

Figure 2.- Continued.

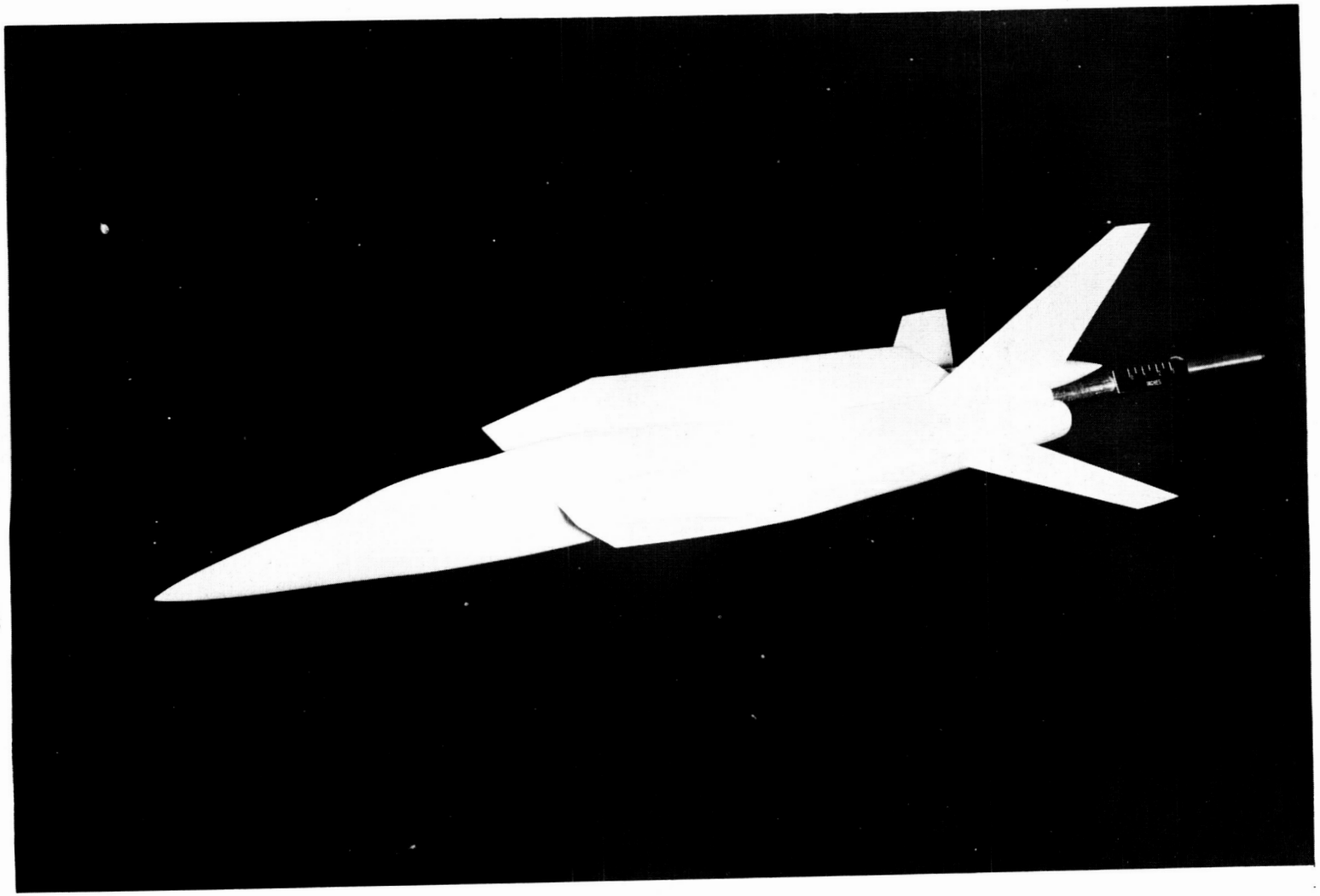

(e) Three-quarter front view. $\Lambda = 94^{\circ}$.

L-60-3169

Figure 2.- Continued.

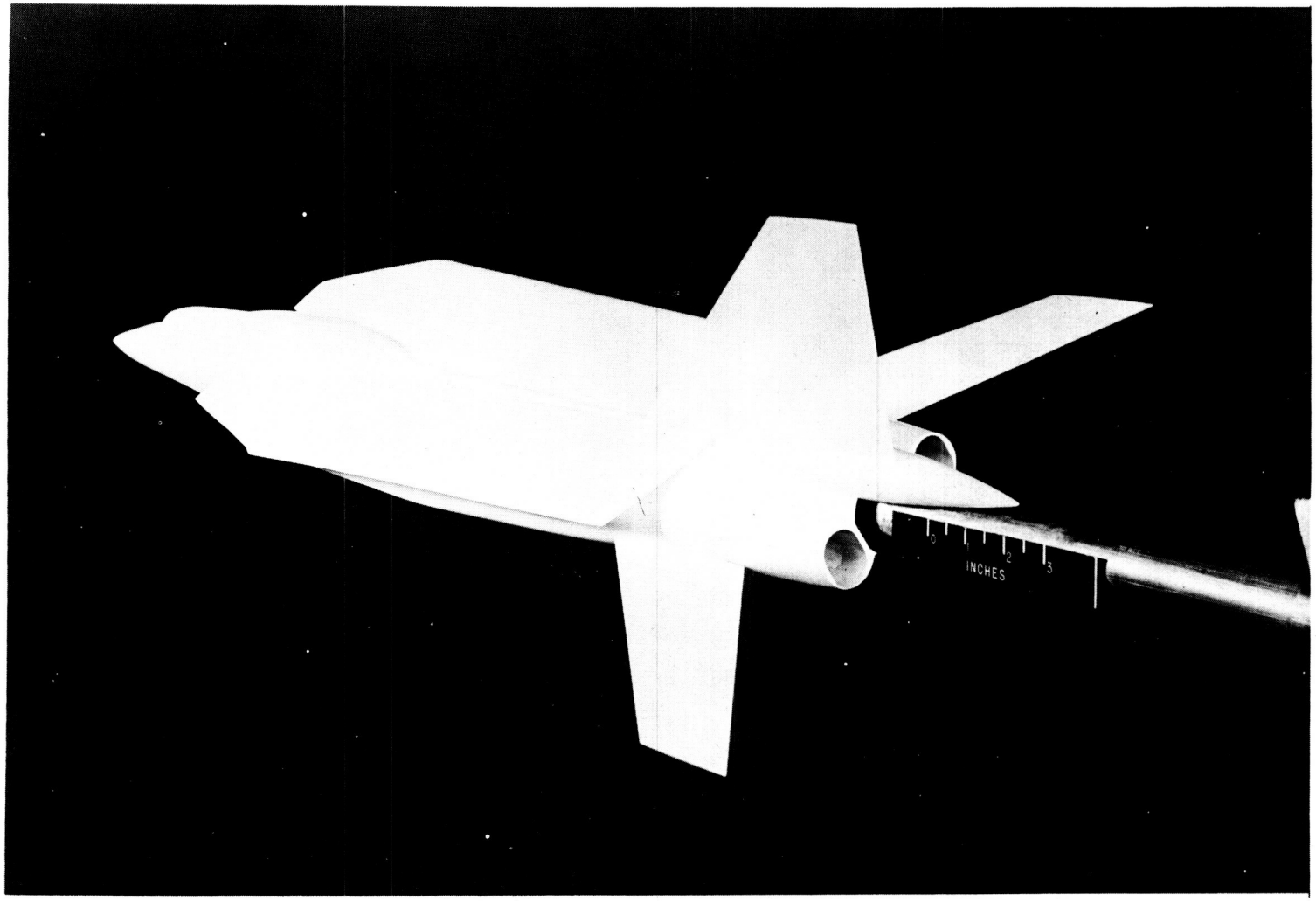

(f) Three-quarter rear view. $\Lambda = 94^{\circ}$. L-60-3171

Figure 2.- Concluded.

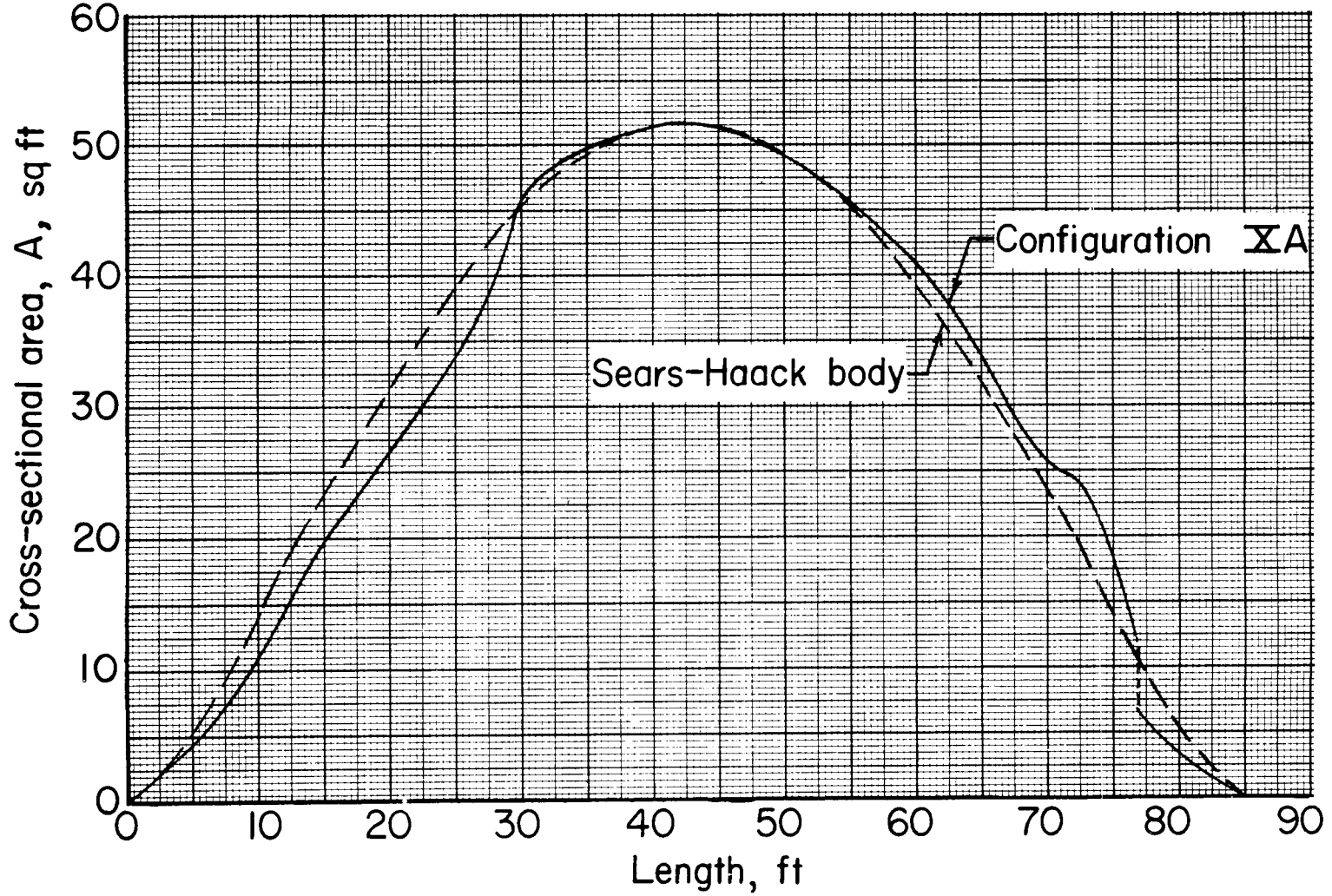

Figure 3.- Longitudinal distribution of cross-sectional area.

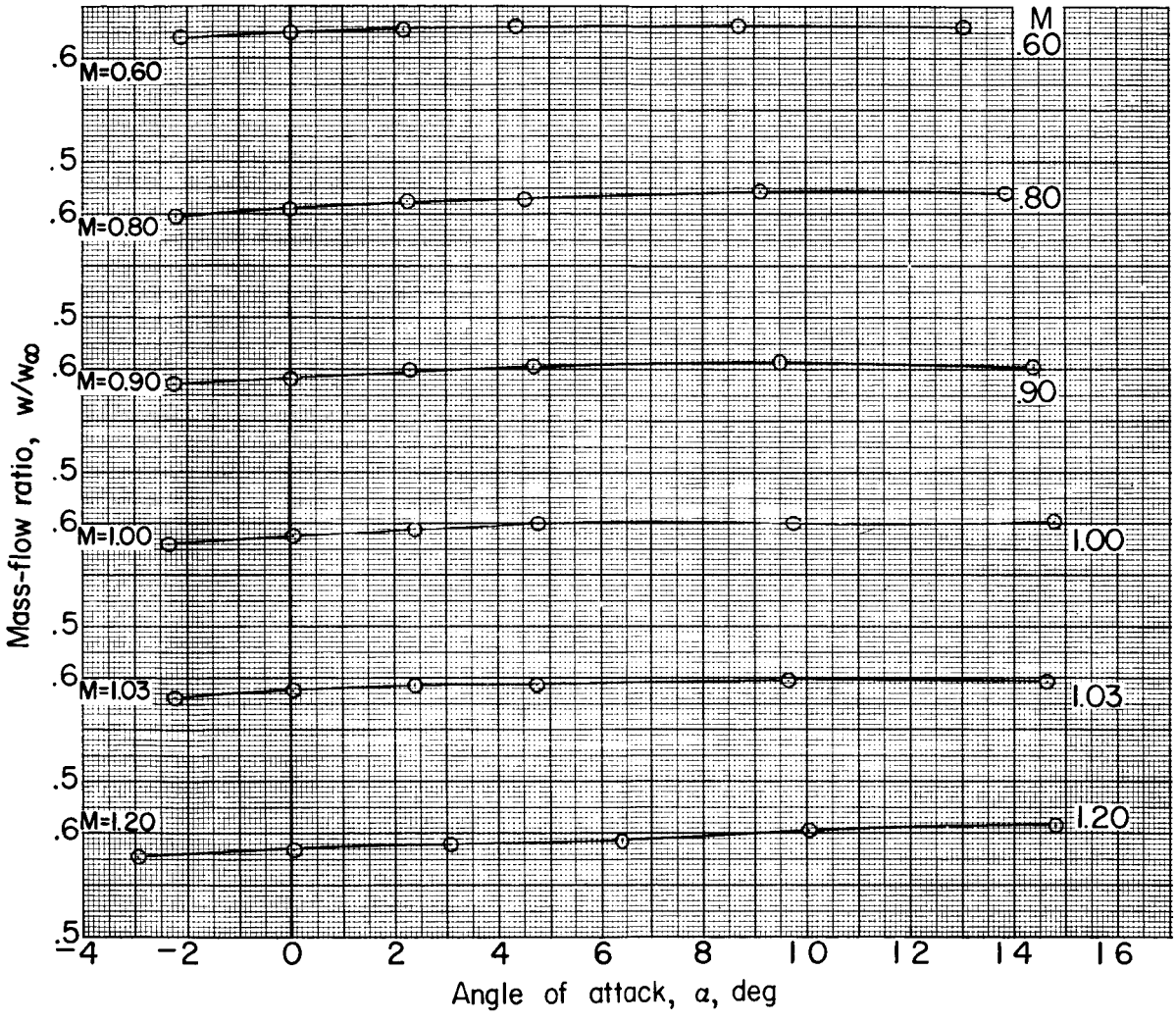

Figure 4.- Variation of mass-flow ratio with angle of attack, based on capture area. A_c = 13.4 square feet, full scale.

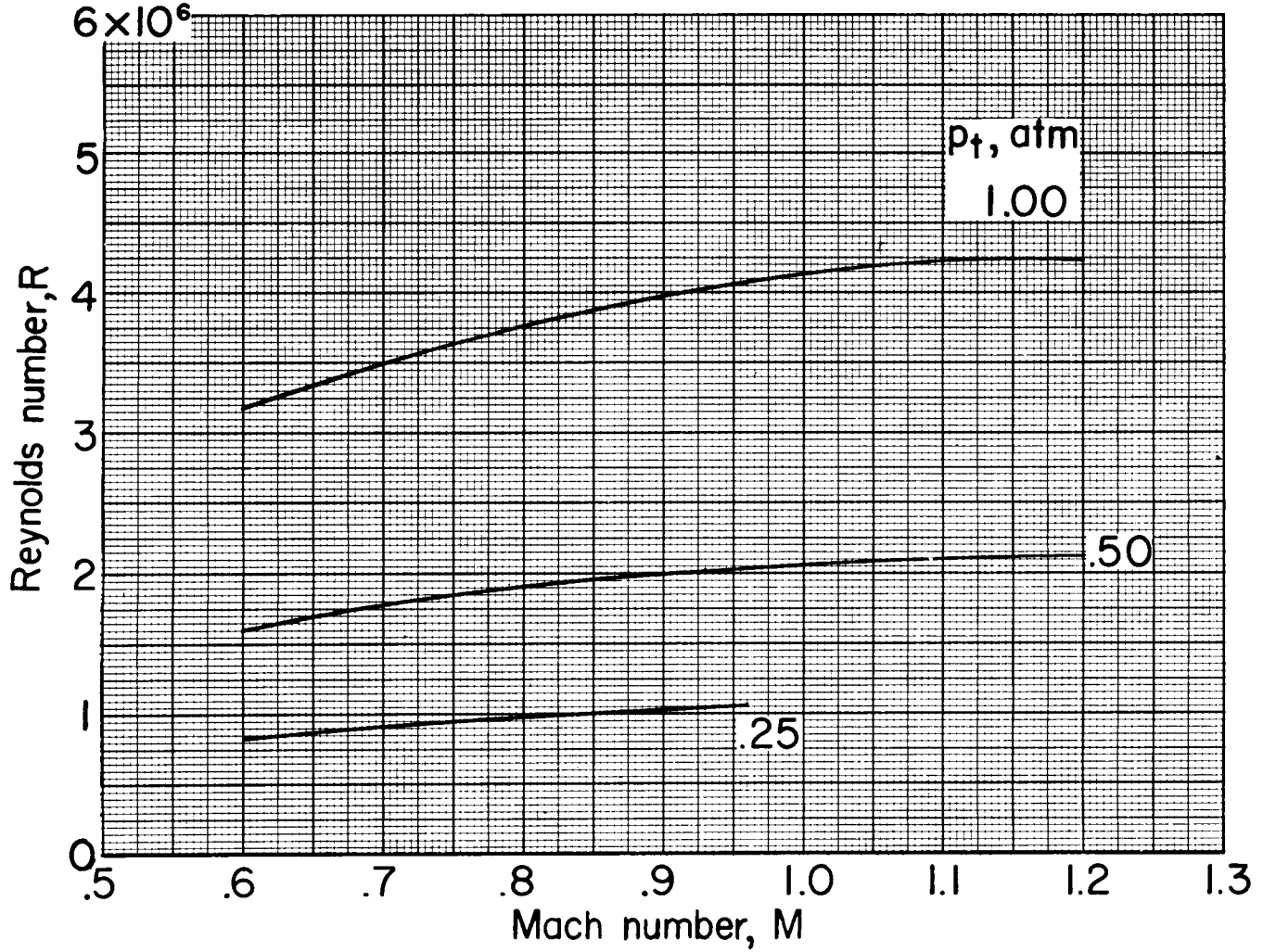

Figure 5.- Variation with Mach number of Reynolds number based on chord of 1 foot.

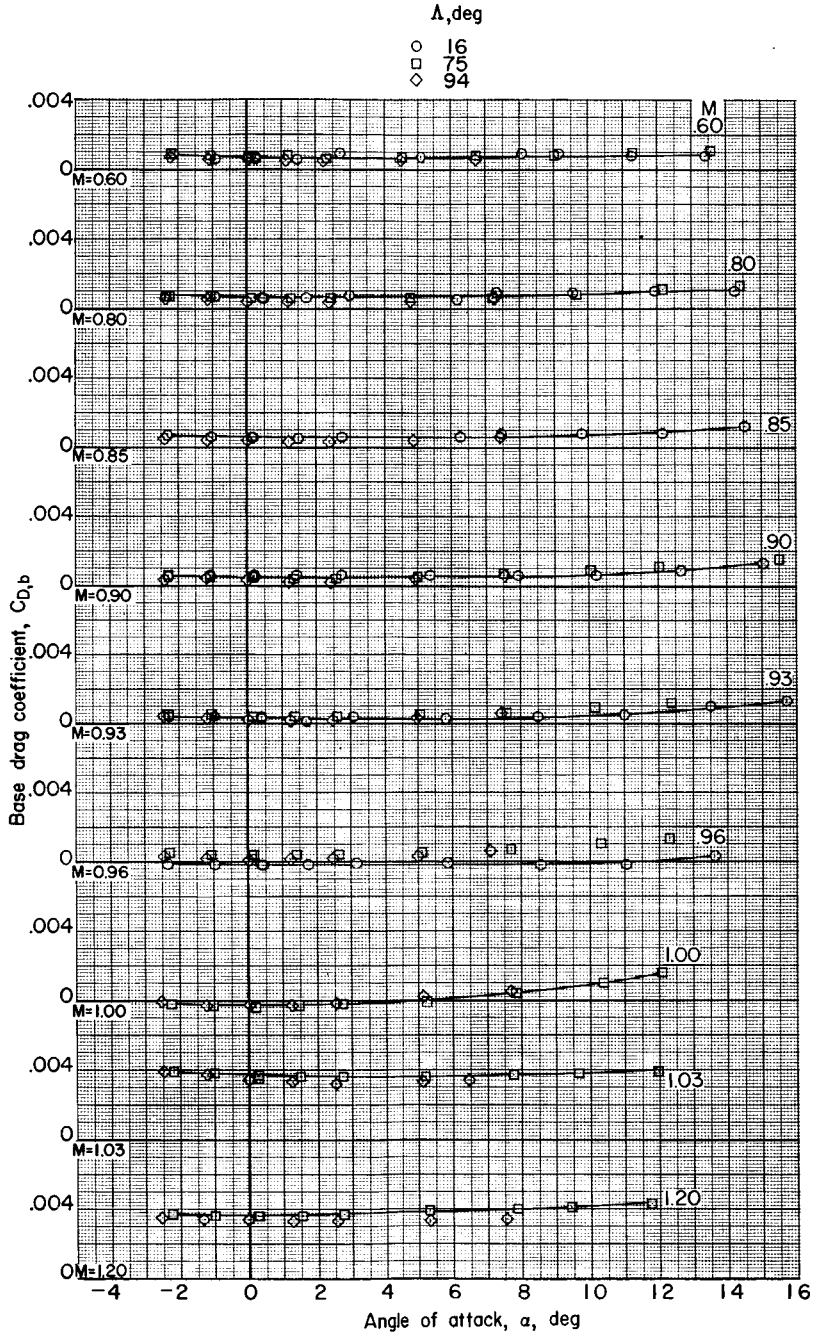

(a) Base drag.

Figure 6.- Variation of base-drag and internal axial-force coefficients with angle of attack.

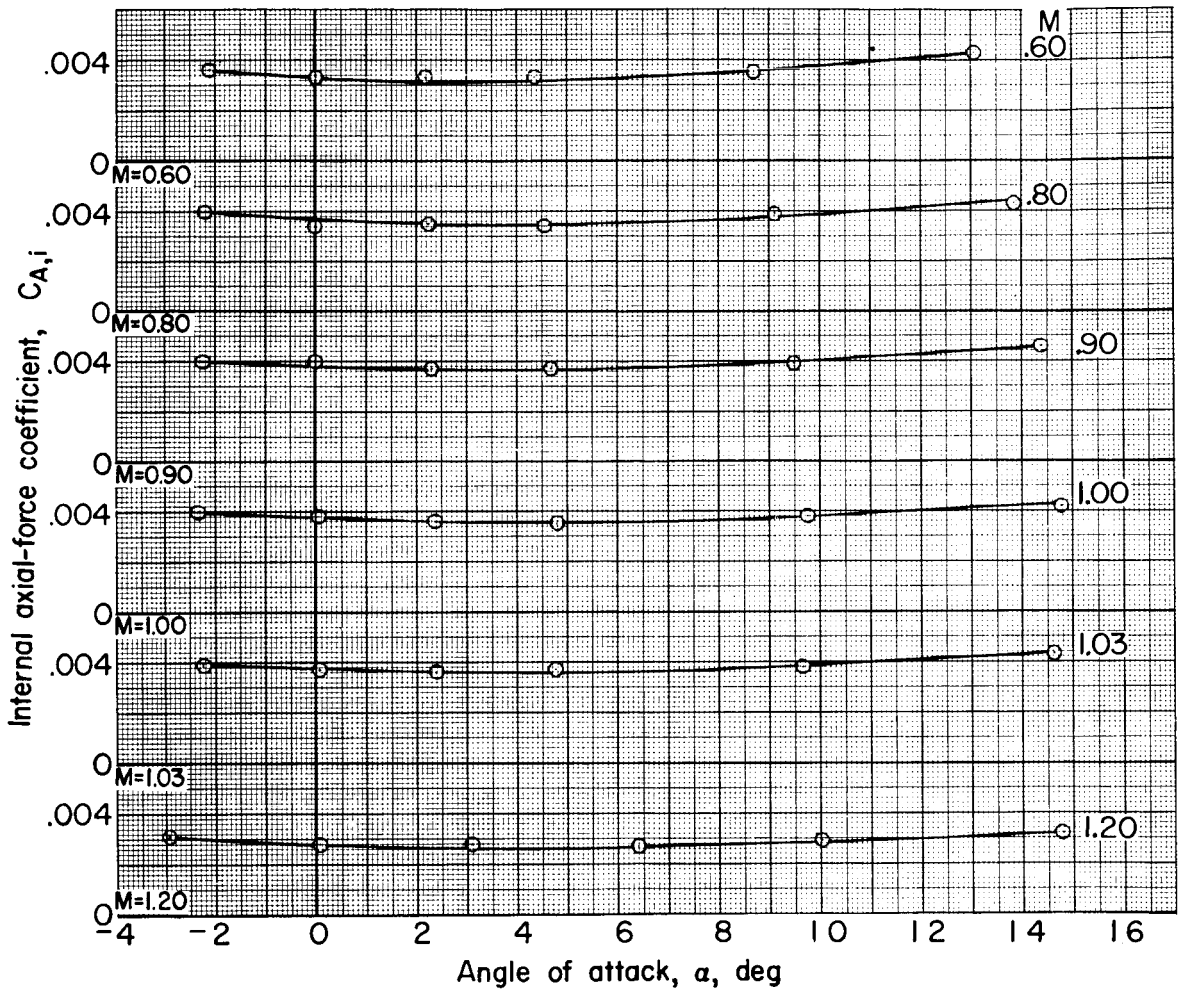

(b) Internal axial force.

Figure 6.- Concluded.

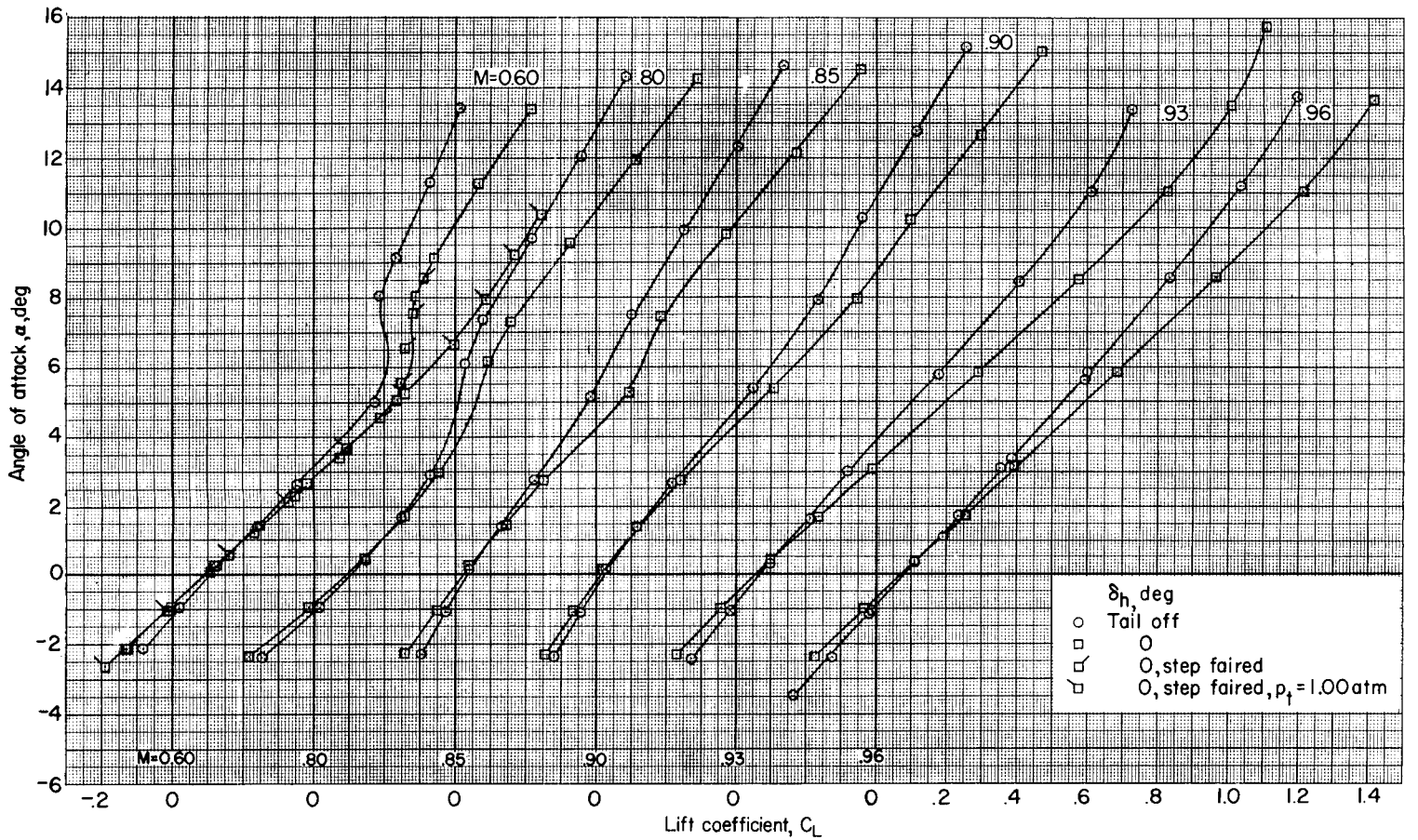

(a) Angle of attack.

Figure 7.- Aerodynamic characteristics of model with wing swept 16°. p_t = 0.25 atmosphere.

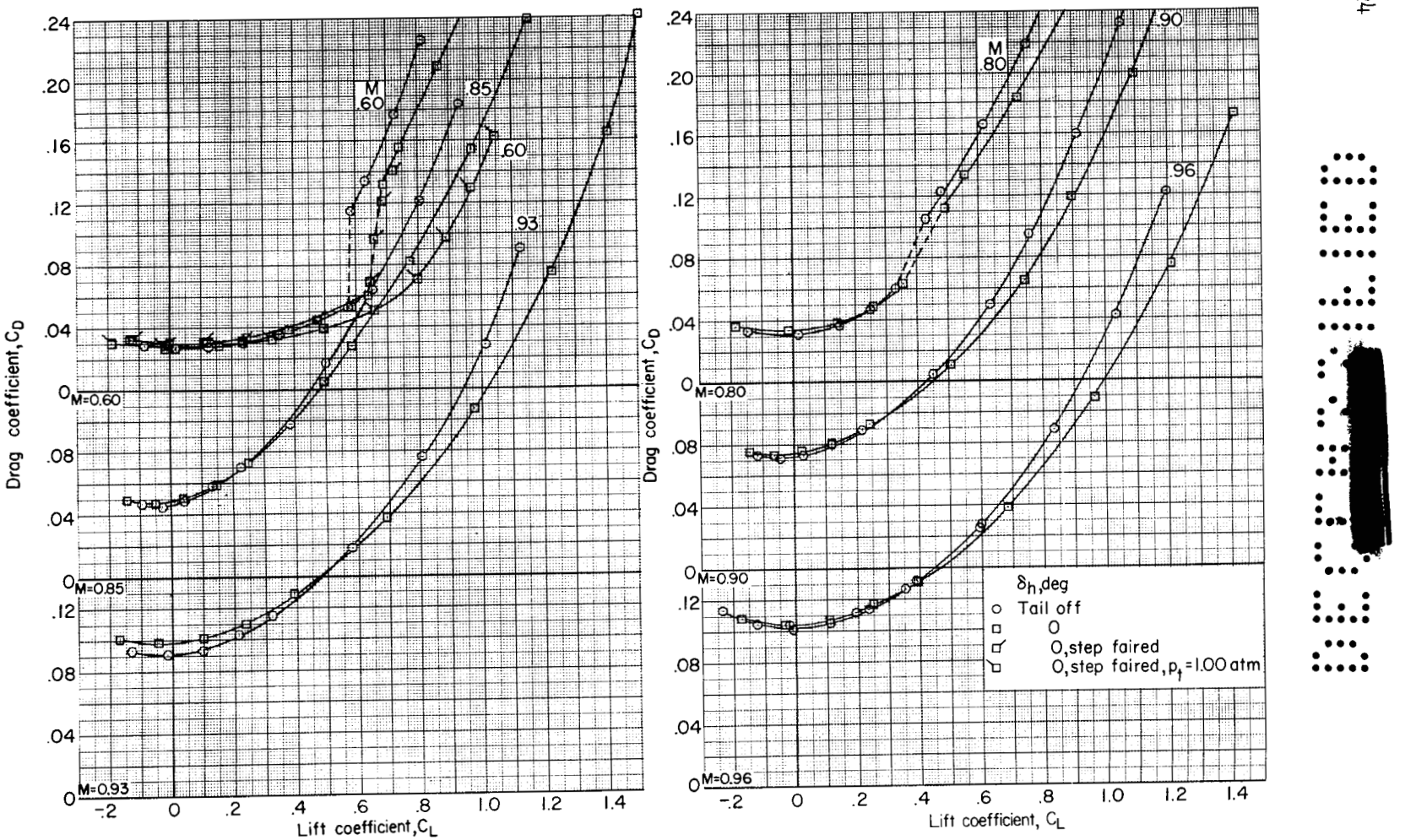

(b) Drag coefficient.

Figure 7.- Continued.

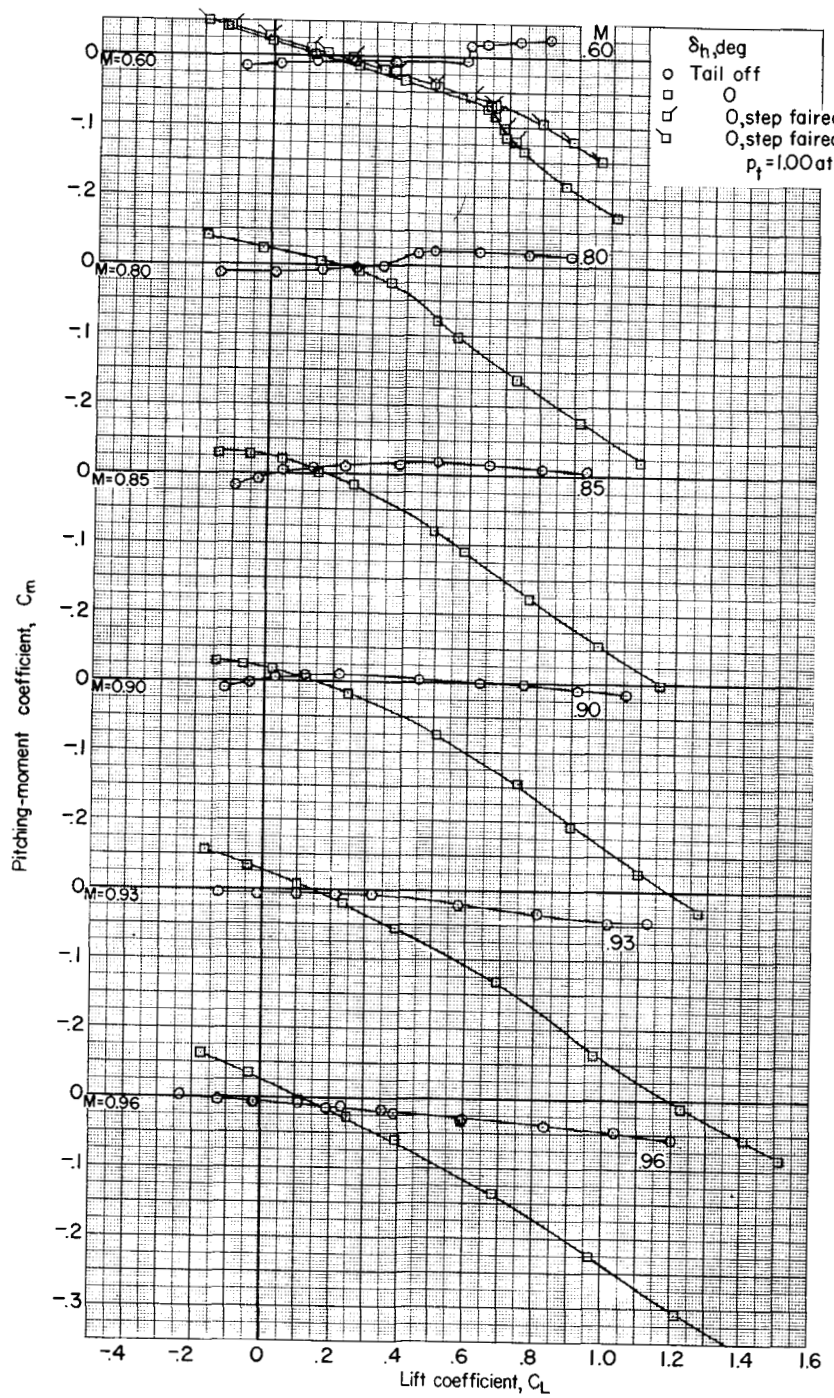

(c) Pitching-moment coefficient.

Figure 7.- Concluded.

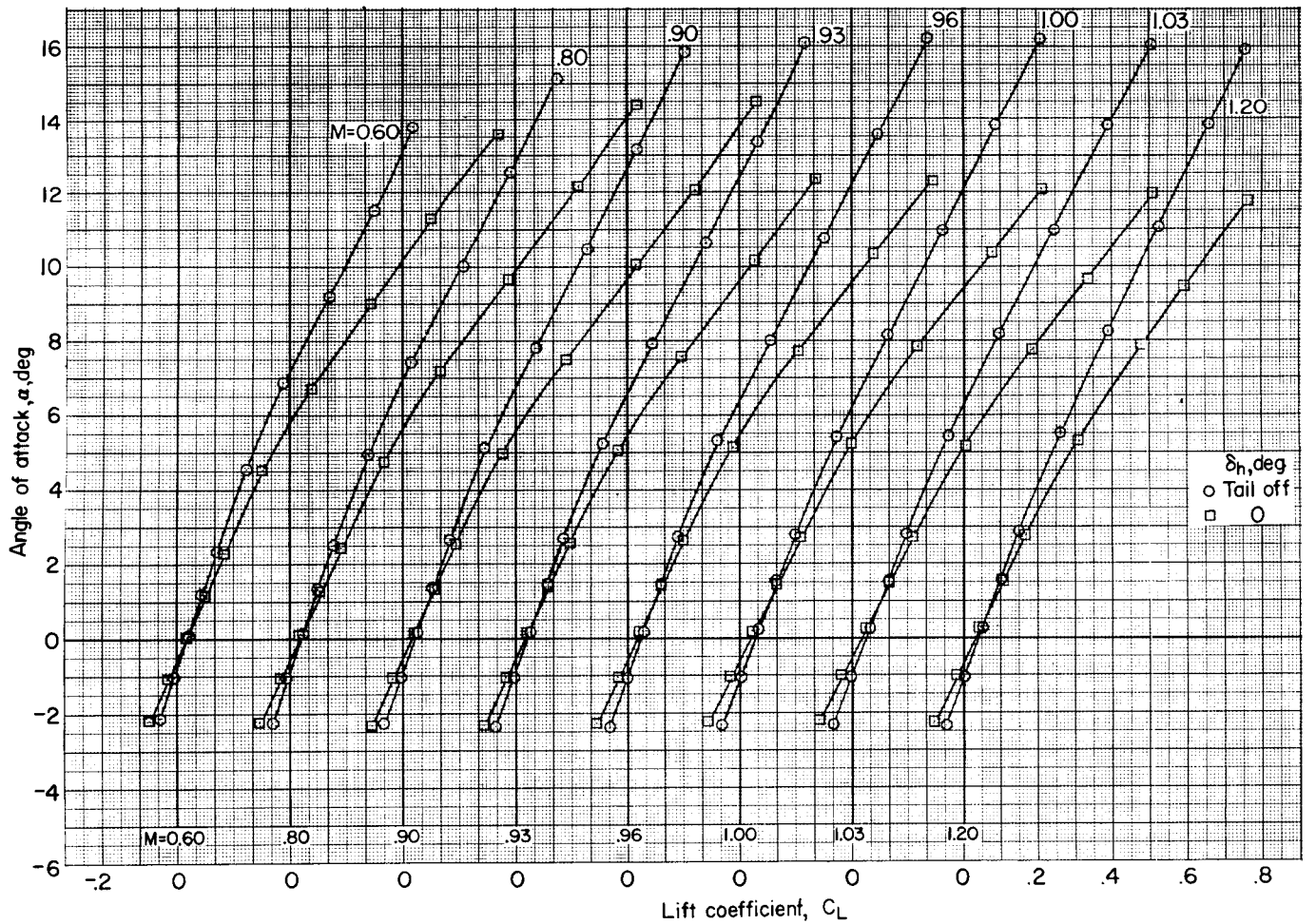

(a) Angle of attack.

Figure 8.- Aerodynamic characteristics of model with wing swept 75°. p_t = 0.50 atmosphere.

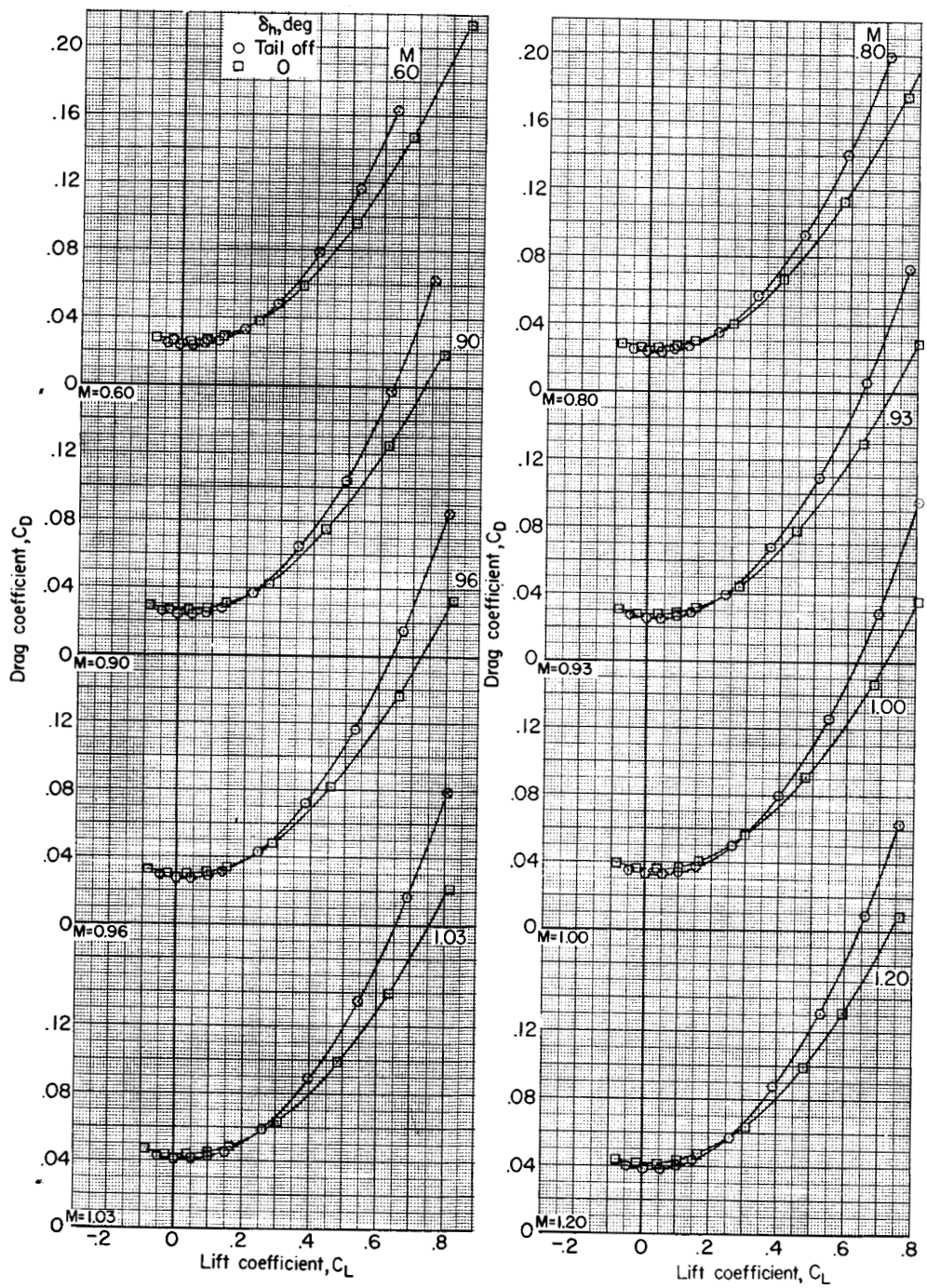

(b) Drag coefficient.

Figure 8.- Continued.

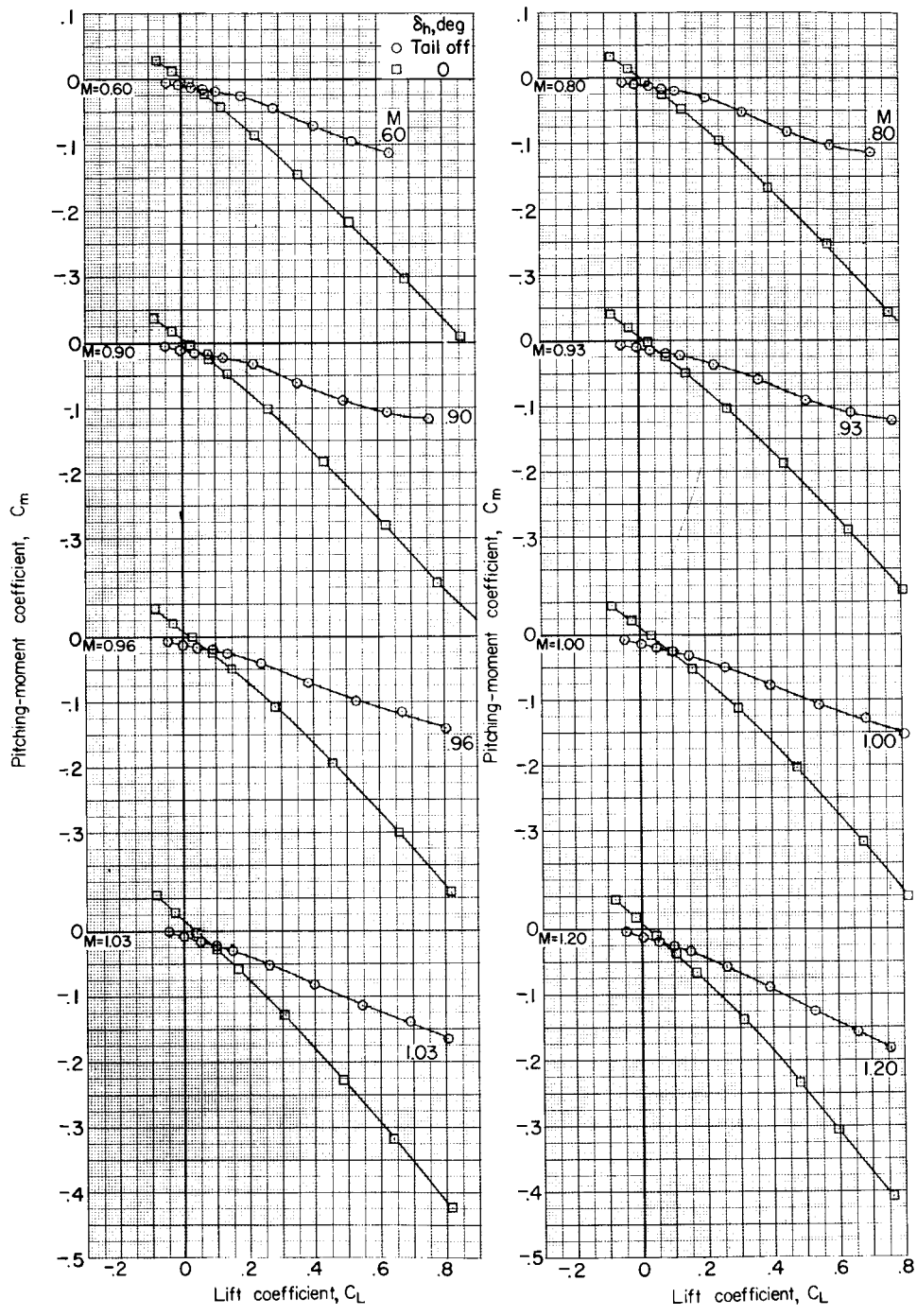

(c) Pitching-moment coefficient.

Figure 8.- Concluded.

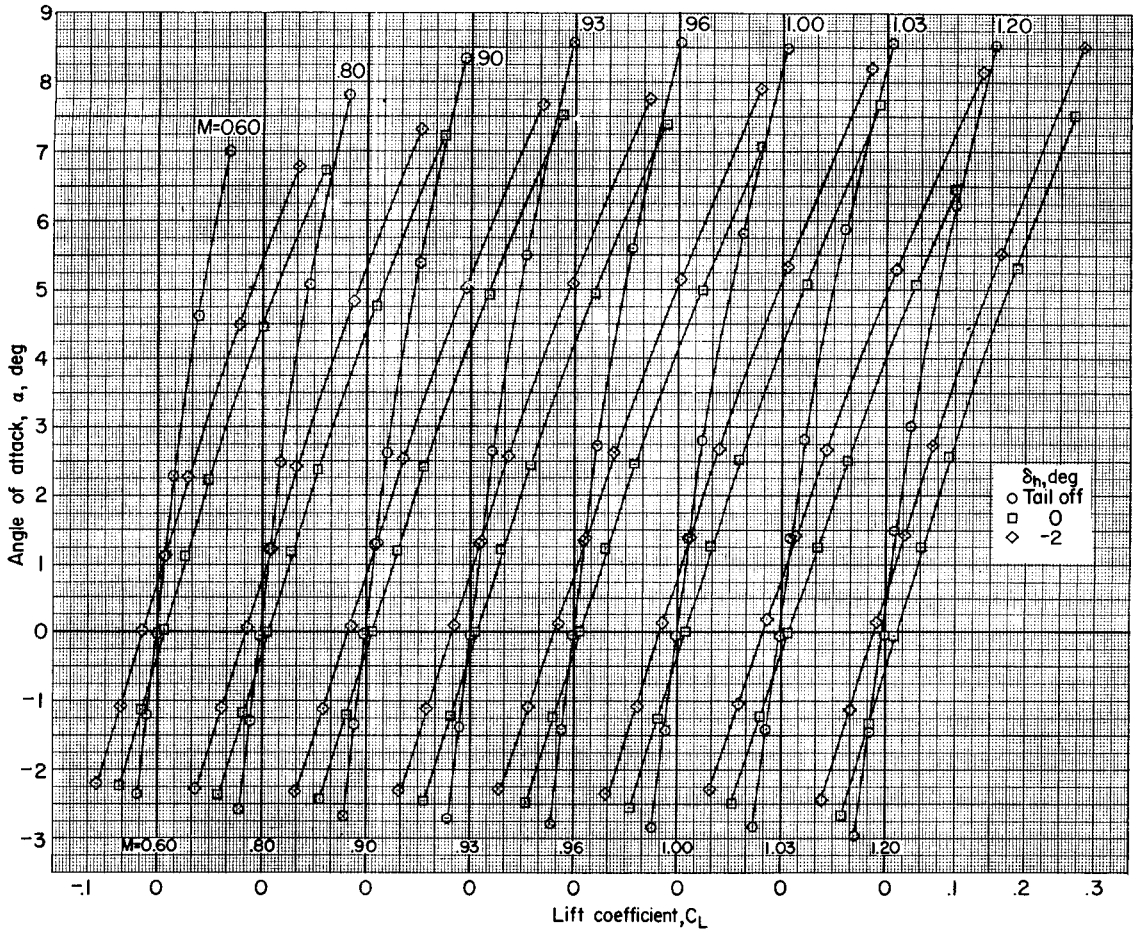

(a) Angle of attack.

Figure 9.- Aerodynamic characteristics of model with wing at maximum sweep. $\Lambda = 94^\circ$; p_t = 1.0 atmosphere.

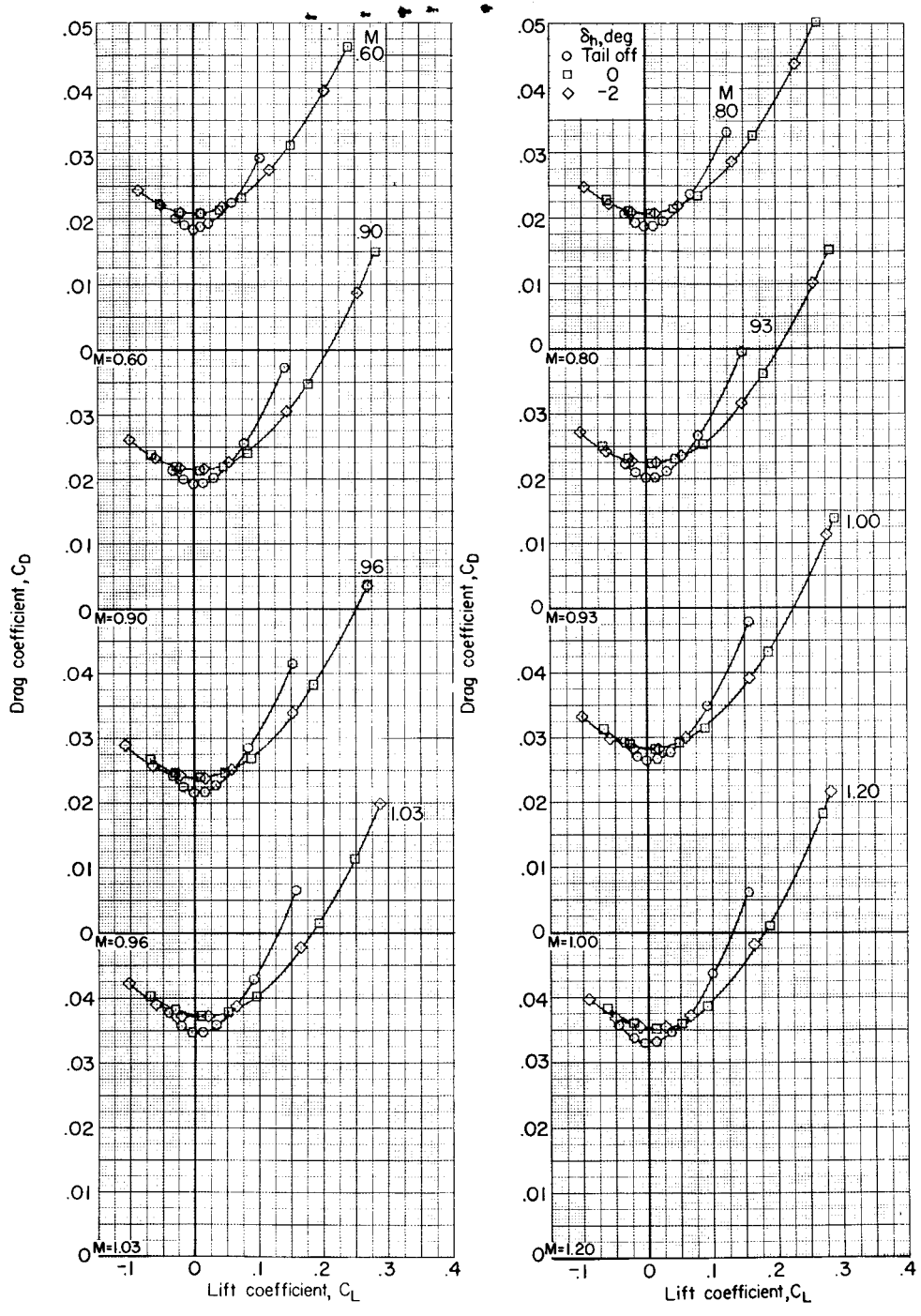

(b) Drag coefficient.

Figure 9.- Continued.

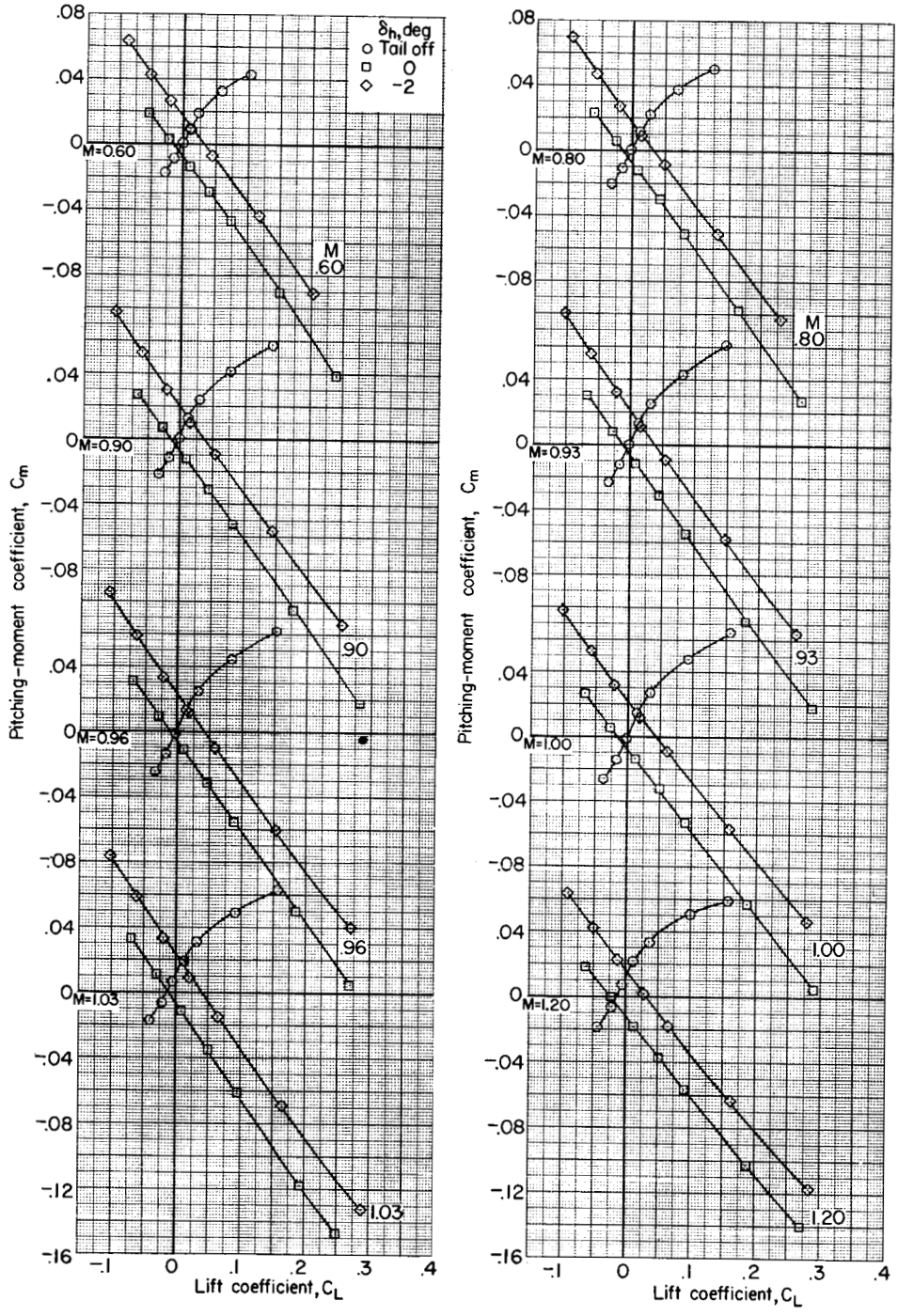

(c) Pitching-moment coefficient.

Figure 9.- Concluded.

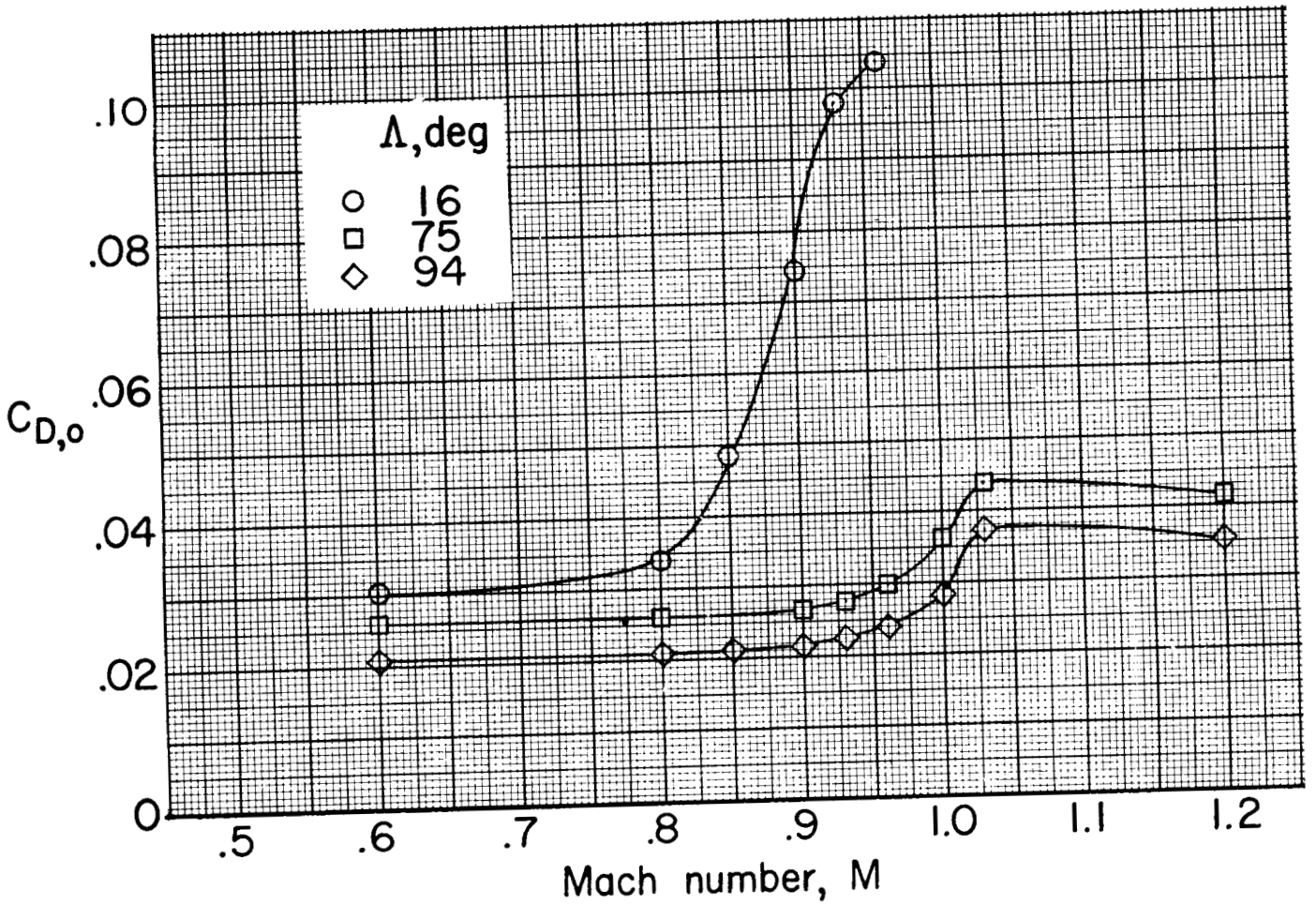

Figure 10.- Comparison of the zero-lift drag for the three wing-sweep angles. $\delta_h = 0^o$.

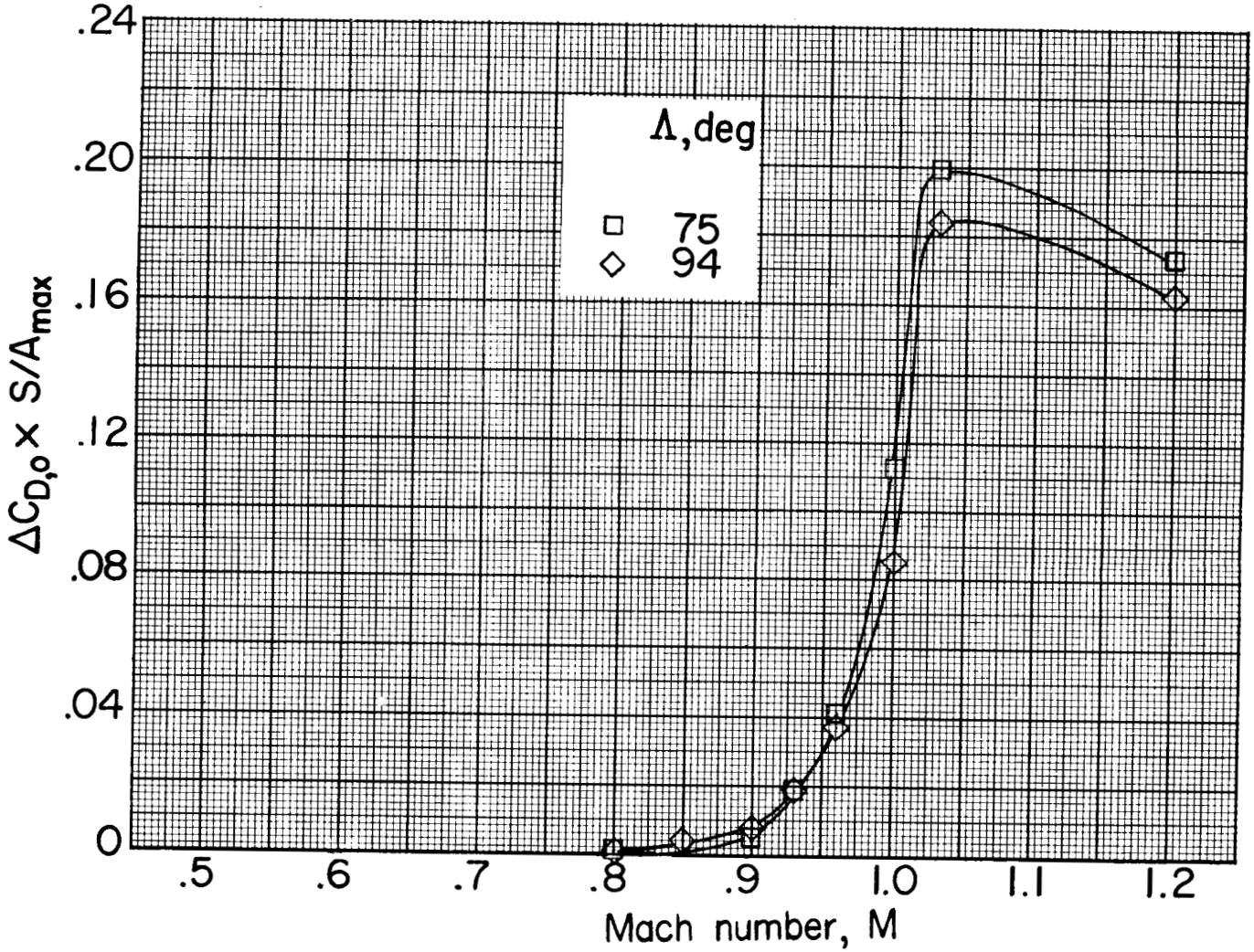

Figure 11.- Variation with Mach number of incremental drag coefficient based on frontal area of 51.7 square feet, full scale. $\delta_h = 0^o$.

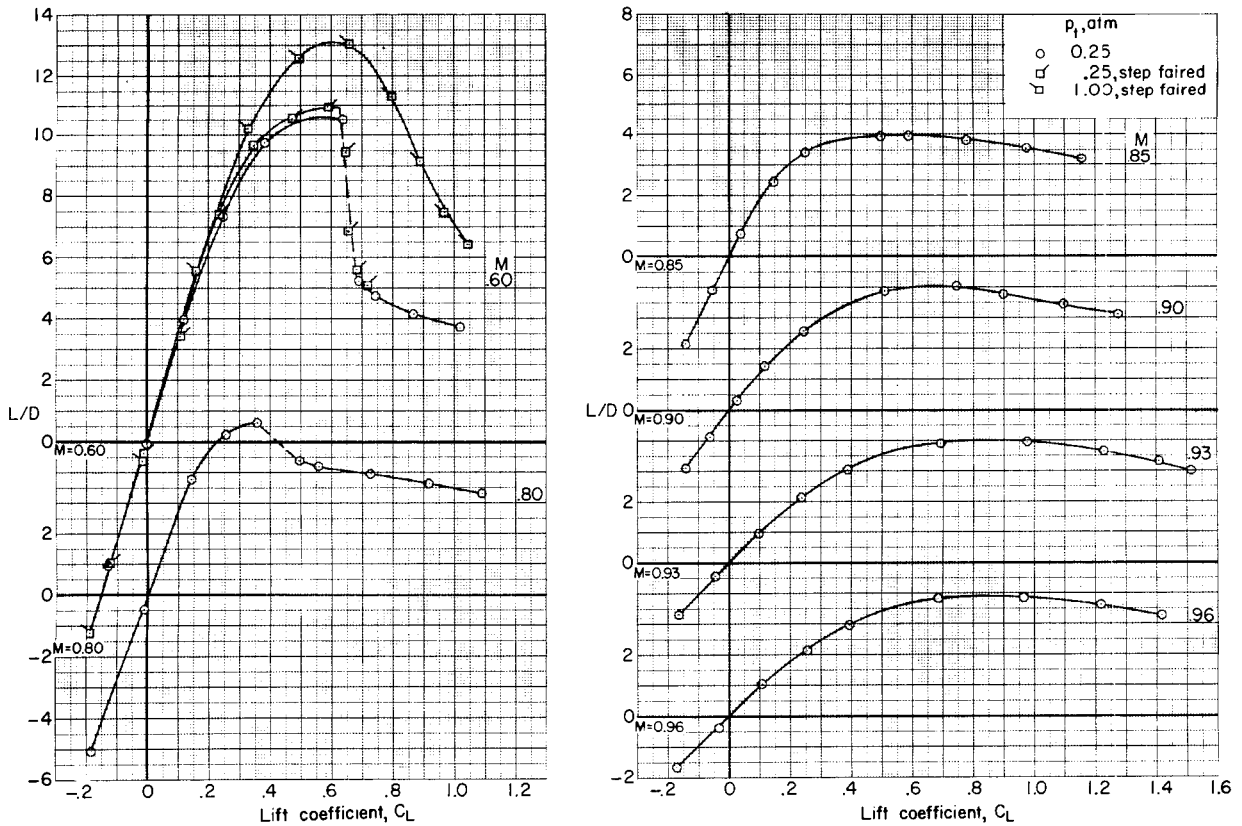

(a) $\Lambda = 16^{\circ}$.

Figure 12.- Variation of the lift-drag ratio with lift coefficient at various Mach numbers.

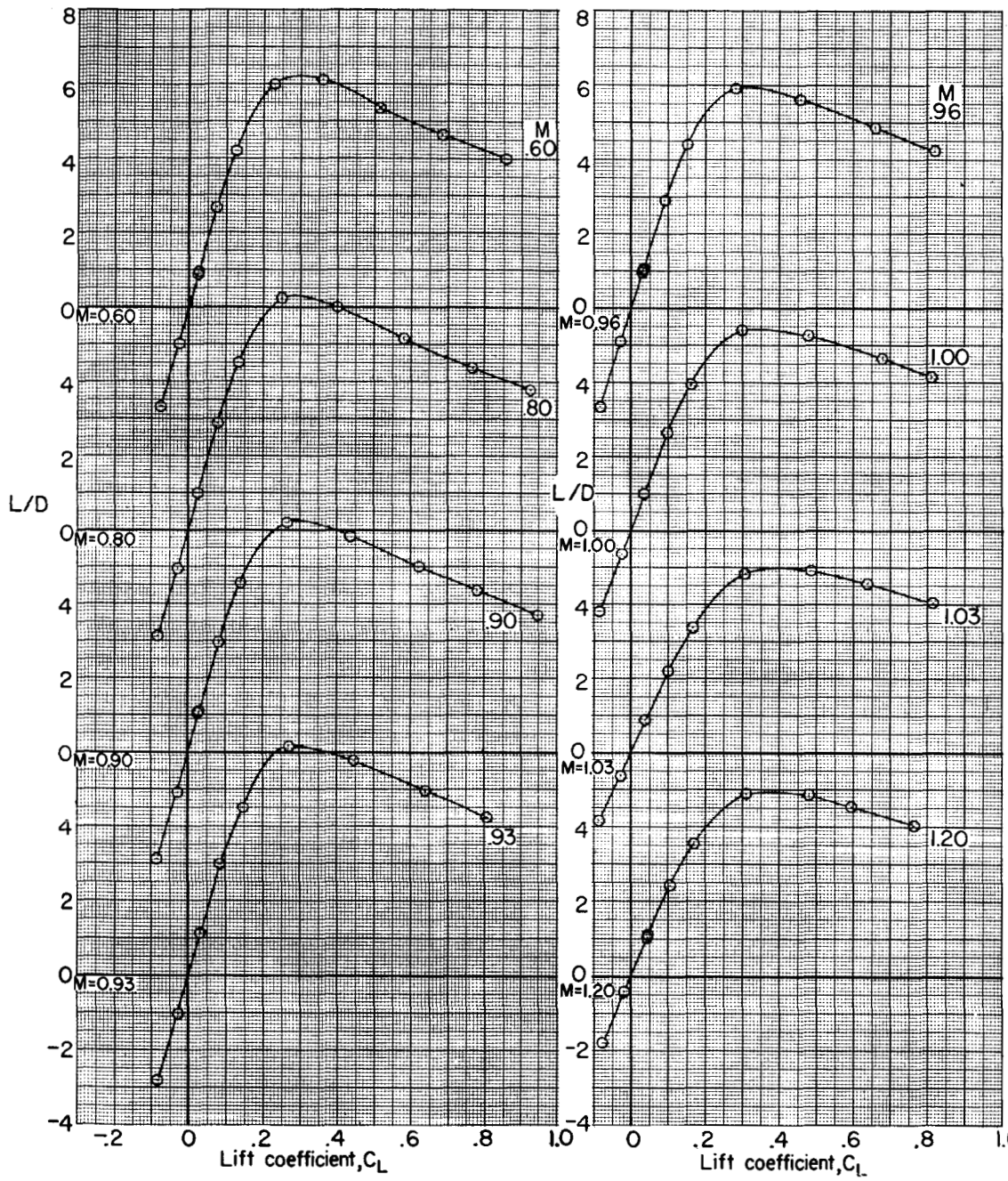

(b) $\Lambda = 75^\circ$.

Figure 12.- Concluded.

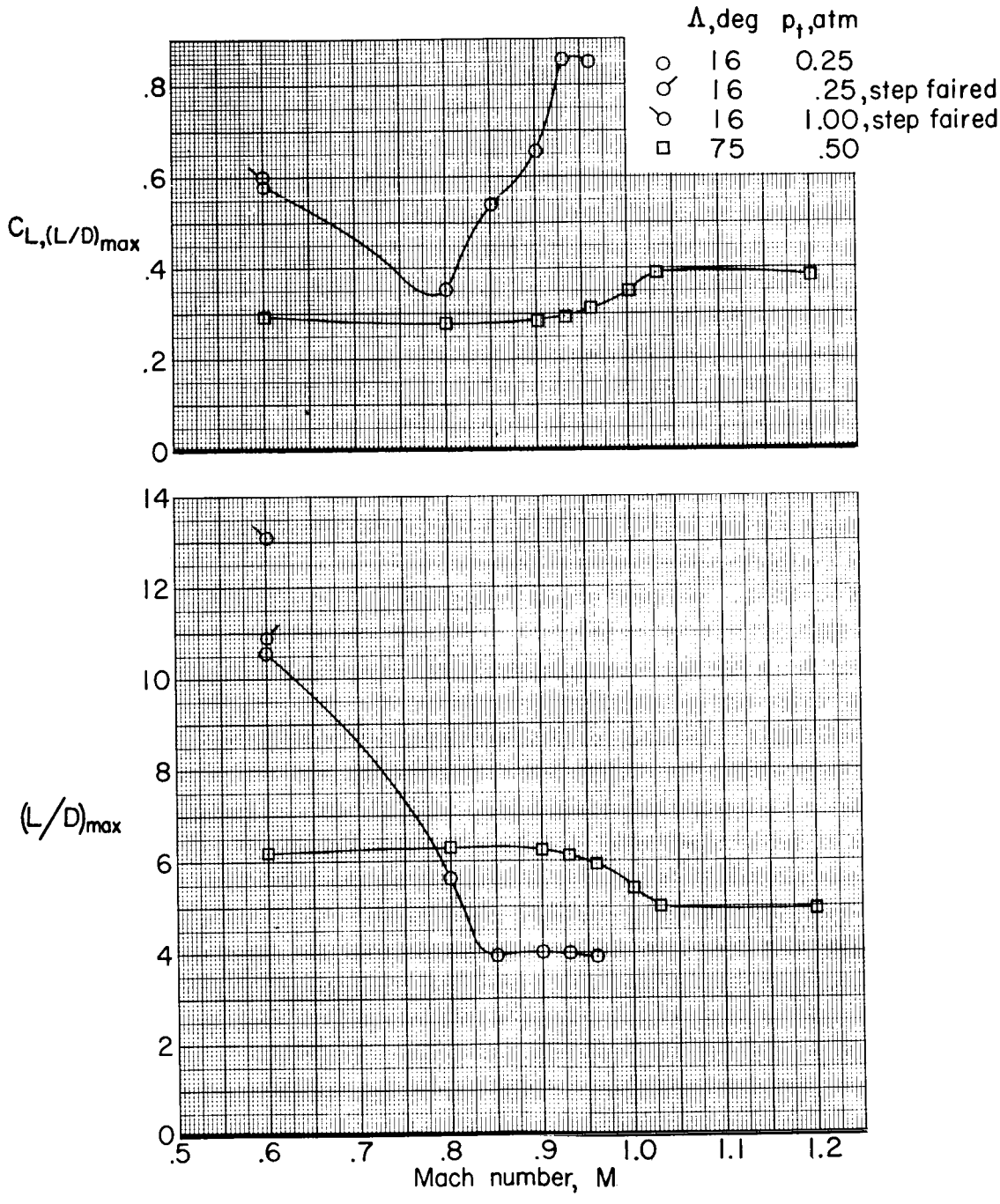

Figure 13.- Variation with Mach number of the maximum lift-drag ratio and lift coefficient for $(L/D)_{max}$.

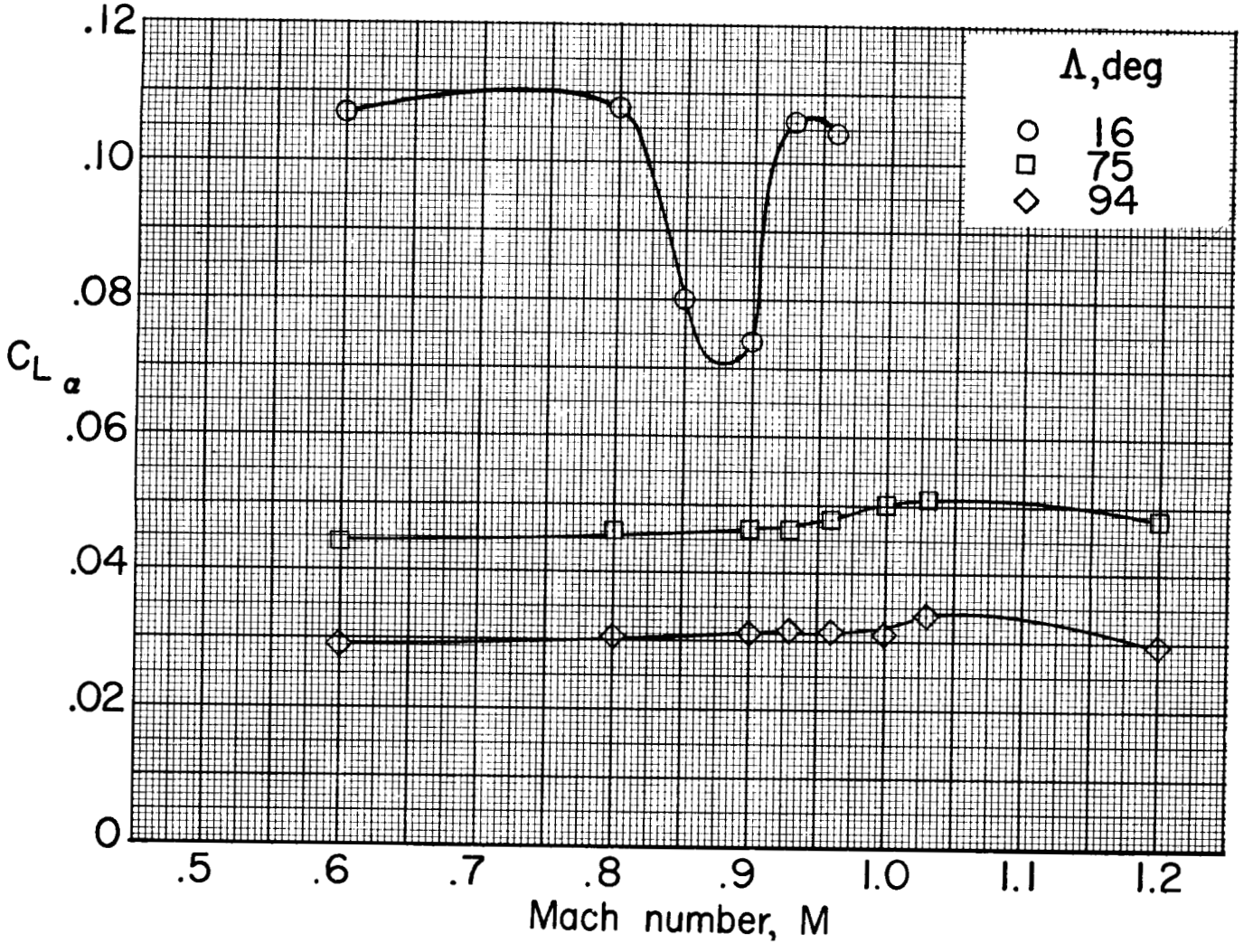

Figure 14.- Comparison of the lift-curve slopes of the configurations with three wing sweeps. $C_L = 0$; $\delta_h = 0^\circ$.

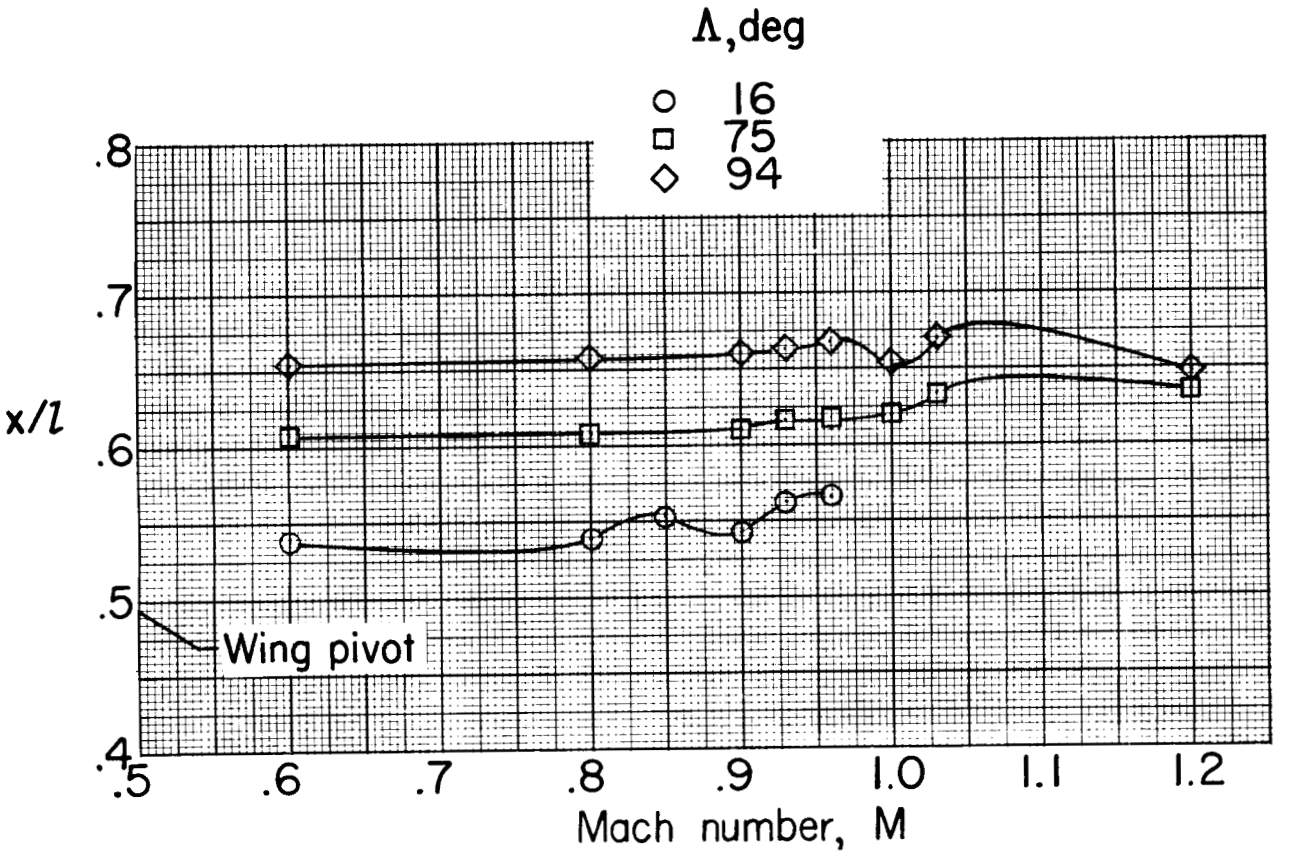

Figure 15.- Variation with Mach number of the aerodynamic-center location for the configurations with three wing sweeps. $C_L = 0$; $\delta_h = 0^\circ$.